Void growth in glassy polymers

Steenbrink, A.C.; van der Giessen, E.; Wu, P.D.

Published in:
Journal of the Mechanics and Physics of Solids

DOI:
10.1016/S0022-5096(96)00093-2

Publication date:
1997

Pergamon

J. Mech. Phys. Solids, Vol. 45, No. 3, pp. 405–437, 1997

0022–5096/97 $17.00 + 0.00

PII: S0022–5096(96) 00093–2

VOID GROWTH IN GLASSY POLYMERS

A. C. STEENBRINK,* E. VAN DER GIESSEN* and P. D. WU†

*Delft University of Technology, Laboratory for Engineering Mechanics, Delft, The Netherlands; and †Université de Sherbrooke, Faculté des Sciences Appliquées, Sherbrooke, Canada

(*Received* 22 *February* 1996; *in revised form* 10 *July* 1996)

ABSTRACT

This paper deals with a study of voids in amorphous glassy polymers that exhibit elastic-viscoplasticity with rate dependent yield, intrinsic softening and progressive strain hardening at large strains. The study is motivated by the plastic deformation in voided polymer–rubber blends caused by cavitation of the rubber particles, and thus attempts to contribute to the understanding of the toughening mechanisms in blends. Axisymmetric cell analyses are presented to study the plastic deformation around initially spherical voids and their resulting growth in terms of size and shape up to large overall strains. This void growth is demonstrated to inherit particular properties from the typical features of plasticity in glassy polymers, viz. small strain softening and large strain hardening. The role of strain localization into shear bands and their subsequent propagation in controlling void growth is highlighted. Furthermore, an approximate constitutive model is presented for the description of the macroscopic overall behaviour of porous glassy polymers. This model includes a modification of existing porous plasticity models to account for elasticity effects on the initiation of overall plasticity, which are important in polymers because of their relatively high yield strain. Its predictions are compared with the results from the numerical cell analyses.

1. INTRODUCTION

In order to increase the toughness of glassy polymers, they are commonly blended with small rubber particles in volume fractions ranging from 20 to 40% [see, e.g., Bucknall, (1977)]. This gives well-known blends such as ABS (acrylonotrile–butadiene–styrene), which is based on the amorphous polymer SAN (styrene–acrylonotrile). While the unmodified parent materials often fail in a brittle manner by crazing, fracture of the blends can occur in a ductile manner (failure strains of SAN are typically no more than 2%, whereas ABS can attain about 30% strain in tension). Owing to intensive experimental research, there is a general consensus that, for many blends, internal cavitation of the rubber particles is the key to toughening. After cavitation, the influence of the relatively soft rubber is negligible, thus leading to an essentially porous material in which plastic deformation is encouraged in the ligaments between voids. This plastic deformation, which in amorphous polymers is due to shear yielding (Argon, 1973), then is primarily responsible for the enhanced energy dissipation that leads to toughening. Thus, the understanding of the initiation of plasticity and the subsequent void growth due to progressive plastic deformation is a critical element in understanding the toughening in many blends.

Because of this importance, the subject of voids in polymers has attracted attention for some time. The first elastic–plastic modelling effort dates back to the analysis of a planar model with cylindrical voids by Haward and Owen (1973), albeit that this was aimed at the problem of craze formation. More recently, similar two-dimensional studies were carried out by, e.g. Sue and Yee (1988) and by Huang and Kinloch (1992), who also briefly considered an axisymmetric model with a spherical void. These studies have delivered important qualitative insights, but the depth of understanding seems to fade in comparison with the understanding of void growth due to plastic flow in ductile metals [see, e.g. Rice and Tracy (1969), Needleman (1972), Tvergaard (1981, 1982), Koplik and Needleman (1988), Hom and McMeeking (1989) and Worswick and Pick (1990)].

At the same time, caution needs to be exercized with transferring results concerning void growth in metals to that in amorphous polymers, due to the almost opposite plastic response. While strain hardening in metals is largest right after yield, plasticity in amorphous polymers is characterized by softening immediately after yield, followed by progressive strain hardening at large deformations (Bowden, 1973). This makes amorphous polymers highly prone to localization of deformation in shear bands at small plastic strains, and at the same time is responsible for large strain phenomena such as neck propagation. At the same time, yielding in polymers is intrinsically dependent on strain-rate, temperature and pressure.

The studies on void growth in polymers referenced above used highly simplistic material models available at the time. Meanwhile, considerable progress has been made in the fully three-dimensional, elastic–viscoplastic constitutive models for amorphous glassy polymers, incorporating rate and temperature dependent plastic flow, including softening and subsequent strain hardening (Boyce *et al.*, 1988, 1992; Wu and Van der Giessen, 1993; Arruda *et al.*, 1995).

The objective of the present paper is two-fold. First of all, a detailed numerical study is carried out of plastic flow around voids and the resulting void growth, using the above-mentioned constitutive models for glassy polymers. This study will make use of an axisymmetric unit cell model for initially spherical voids [corresponding planar studies have been briefly explored by Van der Giessen and Wu (1995) and will be reported further in a forthcoming study]. Particular attention is devoted to the role of localized flow and to the evolution of the void shape. Second, a constitutive model is presented for the description of the macroscopic behaviour of such a porous glassy polymer, and its predictions are compared with the results from the cell analyses. This model draws upon Gurson's (1977) yield function, which is widely applied now for porous metals (Tvergaard, 1990) and has been applied very recently by Lazzeri and Bucknall (1993) and by Jeong and Pan (1995) in relation to polymers; but, we here formulate it in conjunction with the viscoplastic constitutive model referred to earlier and propose a modification to account for the influence of elasticity which is quite significant in polymers due to the fact that the strain at yield is relatively large (typically around 5%).

The presentation uses tensor notation where tensors are denoted by bold-face symbols, $\otimes$ is the tensor product and $\cdot$ the scalar product. For example, with respect to a Cartesian basis $\mathbf{e}_i$, $\mathbf{AB} = A_{ik}B_{kj}\mathbf{e}_i \otimes \mathbf{e}_j$, $\mathbf{A}\cdot\mathbf{B} = A_{ij}B_{ij}$ and $\mathscr{L}\mathbf{B} = \mathscr{L}_{ijkl}B_{kl}\mathbf{e}_i \otimes \mathbf{e}_j$, with summation implied over repeated Latin indices. The summation convention is

not used for repeated Greek indices. A prime ()′ identifies the deviatoric part of a second-order tensor, and tr denotes the trace.

2. CONSTITUTIVE MODEL

The large strain behaviour of amorphous glassy polymers is characterized by strain-rate dependent yield, followed immediately by intrinsic strain softening and subsequently followed by the development of increasing strain hardening. The strain softening is inseparably connected with yielding by way of the molecular mechanisms of macroscopic yielding (Bowden, 1973). On a sufficiently small, microscopic scale, yielding is accompanied by the occurrence of multiple fine shear or slip bands, and for this reason the phenomenon is usually referred to as "shear yielding". The increasing strain hardening is associated with the stretching of the molecular network between entanglements and the simultaneous development of a preferred orientation of the molecular chains.

Haward and Thackray (1968) proposed a pioneering, one-dimensional model that incorporates the mentioned deformation mechanisms for plasticity on a macroscopic scale. Recently, Boyce *et al.* (1988) generalized this model to general three-dimensional deformations. Yielding in this theory is described in terms of macroscopic plastic flow governed by a constitutive relation developed by Argon (1973), and the description for orientational hardening draws on an analogy with rubber elasticity. Softening is characterized by a simple phenomenological evolution law. Several refinements of the Boyce *et al.* (1988) model have been proposed since; here, we use the model in the same form as we used in previous studies (Wu and Van der Giessen, 1994, 1995a, b). In the following, we only give a brief summary of the constitutive equations.

Confining attention to isothermal situations and assuming the elastic strains to remain small, the material model is based on an additive decomposition of the rate of deformation $\mathbf{D}$ into an elastic part $\mathbf{D}^e$ and a plastic part $\mathbf{D}^p$

$$\mathbf{D} = \mathbf{D}^e + \mathbf{D}^p, \tag{1}$$

where the elastic part of the response is taken to be governed by the hypoelastic law

$$\mathbf{D}^e = \mathscr{L}_e^{-1} \overset{\nabla}{\boldsymbol{\sigma}} \tag{2}$$

in terms of the Jaumann derivative, $\overset{\nabla}{\boldsymbol{\sigma}} = \dot{\boldsymbol{\sigma}} - \mathbf{W}\boldsymbol{\sigma} + \boldsymbol{\sigma}\mathbf{W}$ of the Cauchy stress tensor $\boldsymbol{\sigma}$ based on the continuum spin tensor $\mathbf{W}$. Here, $\mathscr{L}_e$ is the standard fourth-order isotropic elastic modulus tensor with Cartesian components

$$\mathscr{L}_{ijkl} = \frac{E}{2(1+\nu)}\left[(\delta_{ik}\delta_{jl} + \delta_{il}\delta_{jk}) + \frac{2\nu}{1-2\nu}\delta_{ij}\delta_{kl}\right], \tag{3}$$

in terms of Young's modulus E and Poisson's ratio ν.

The plastic strain rate $\mathbf{D}^p$ is taken to be specified through the viscoplastic constitutive equation

$$D^{\mathrm{p}} = \frac{\dot{\gamma}^{\mathrm{p}}}{\sqrt{2}\tau}\bar{\boldsymbol{\sigma}}', \tag{4}$$

where τ is the equivalent shear stress

$$\tau = \sqrt{\tfrac{1}{2}\bar{\boldsymbol{\sigma}}' \cdot \bar{\boldsymbol{\sigma}}'}, \tag{5}$$

specified in terms of the deviatoric part $\bar{\boldsymbol{\sigma}}'$ of the driving stress

$$\bar{\boldsymbol{\sigma}} = \boldsymbol{\sigma} - \mathbf{b}.$$

The back stress tensor $\mathbf{b}$ describes the orientational hardening of the material, and will be further specified later. The equivalent plastic shear strain rate $\dot{\gamma}^{\mathrm{p}}$ in (4)

$$\dot{\gamma}^{\mathrm{p}} = \sqrt{\mathbf{D}^{\mathrm{p}} \cdot \mathbf{D}^{\mathrm{p}}}, \tag{6}$$

is given by the expression (Argon, 1973)

$$\dot{\gamma}^{\mathrm{p}} = \dot{\gamma}_0 \exp\left[-\frac{As_0}{T}\left(1-\left(\frac{\tau}{s_0}\right)^{5/6}\right)\right], \tag{7}$$

where $\dot{\gamma}_0$ and A are material parameters, T is the absolute temperature, and s_0 is the shear strength. In order to incorporate the effect of the pressure p on plastic flow in glassy polymers, s_0 in (7) is replaced with $s_0+\alpha p$. Furthermore, the effect of strain softening is incorporated by using a plastic shear dependent shear strength s instead of s_0, governed by

$$\dot{s} = h(1-s/s_{\mathrm{ss}})\dot{\gamma}^{\mathrm{p}}. \tag{8}$$

The saturation value of s is s_{ss}, while α and h are additional material parameters. The plastic dissipation per unit volume is given by

$$\bar{\boldsymbol{\sigma}}' \cdot \mathbf{D}^{\mathrm{p}} = \sqrt{2}\tau\dot{\gamma}^{\mathrm{p}},$$

but, as mentioned before, the associated temperature rise has been ignored in this study.

The description of the strain hardening in amorphous polymers makes use of the analogy with the stretching of the cross-linked network in rubbers (Boyce *et al.*, 1988). The constitutive equations for the back stress tensor $\mathbf{b}$ are formulated through a functional description of its principal components b_α on the unit principal directions $\mathbf{e}_\alpha^p$ of the left plastic stretch tensor, in terms of the corresponding principal plastic stretches λ_α, i.e.

$$\mathbf{b} = \sum_\alpha b_\alpha(\mathbf{e}_\alpha^{\mathrm{p}} \otimes \mathbf{e}_\alpha^{\mathrm{p}}), b_\alpha = b_\alpha(\lambda_\beta).$$

Here, to avoid confusion, principal tensor components and the corresponding eigenvectors are denoted with Greek indices, for which the summation convention is not implied. When the elastic deformations remain small, the plastic stretches can be approximated by the total stretches (Wu and Van der Giessen, 1996). The constitutive model used here was proposed by Wu and Van der Giessen (1993) on the basis of their description of the fully three-dimensional orientation distribution of molecular

chains in a non-Gaussian network. They showed that their numerical computations for such a network can be captured very accurately by the following combination of the classical three-chain network description and the Arruda and Boyce (1993) eight-chain model

$$b_\alpha = (1-\rho)b_\alpha^{3-\mathrm{ch}} + \rho b_\alpha^{8-\mathrm{ch}}, \tag{9}$$

with ρ being determined by the maximum plastic stretch $\bar{\lambda} = \max(\lambda_1, \lambda_2, \lambda_3)$ through $\rho = 0.85\bar{\lambda}/\sqrt{N}$. Here, N is a statistical network parameter, which gives the average number of links between entanglements (or cross-links in a rubber) and thus determines the limit stretch $\lambda_{\max}$ of a molecular chain as $\lambda_{\max} = \sqrt{N}$. The principal back stress components $b_\alpha^{3-\mathrm{ch}}$ and $b_\alpha^{8-\mathrm{ch}}$ are given by

$$b_\alpha^{3-\mathrm{ch}} = \frac{1}{3}C^{\mathrm{R}}\sqrt{N}\lambda_\alpha \mathscr{L}^{-1}\left(\frac{\lambda_\alpha}{\sqrt{N}}\right), \tag{10}$$

$$b_\alpha^{8-\mathrm{ch}} = \frac{1}{3}C^{\mathrm{R}}\sqrt{N}\frac{\lambda_\alpha^2}{\lambda_{\mathrm{c}}}\mathscr{L}^{-1}\left(\frac{\lambda_{\mathrm{c}}}{\sqrt{N}}\right); \quad \lambda_{\mathrm{c}}^2 = \frac{1}{3}\sum_{\beta=1}^{3}\lambda_\beta^2, \tag{11}$$

where $\mathscr{L}$ denotes the Langevin function defined as

$$\mathscr{L}(\beta) = \coth\ \beta - 1/\beta.$$

In the theory of rubber elasticity, the material parameter C^{R} is termed the rubbery modulus. When the value of either $\bar{\lambda}$ or λ_{c} approaches $\lambda_{\max}$, the hardening rate increases dramatically, thereby suppressing effectively all further plastic flow, and the network locks. Therefore, for monotonic loading conditions, when either λ_α or λ_{c} exceeds the value $0.99\lambda_{\max}$, the network is "locked" and no further viscoplastic flow is allowed.

3. PROBLEM FORMULATION AND METHOD OF ANALYSIS

Similar to the study by Koplik and Needleman (1988), the behaviour of the porous material is investigated in terms of an axisymmetric unit cell model, illustrated in Fig. 1. In the initial, undeformed configuration, the unit cell is a cylinder with radius b_0 and height $2h_0$. The voids are assumed to be spherical initially, with radius a_0, so that the initial void volume fraction is $f_0 = \frac{2}{3}a_0^3/(b_0^2 h_0)$. The deformations of the cell are monitored by means of a convective coordinate system that initially coincides with a cylindrical coordinate system with radial coordinate x^1, axial coordinate x^2 and circumferential coordinate x^3. During the finite strain deformation process, the cell remains a cylinder, characterized in an arbitrary state by a radius $b = b_0 + U_1$ and height $h = h_0 + U_2$, with radial and axial displacements U_1 and U_2, respectively.

The material is presumed to be remotely loaded by an axisymmetric stress state with a macroscopic true stress Σ_2 in the x^2-direction, and true stress Σ_1 in x^1 and x^3-directions (see Fig. 1). In all cases, the x^2-direction is assumed to be the maximum principal stress direction. The corresponding macroscopic logarithmic strains are E_2 and E_1, respectively,

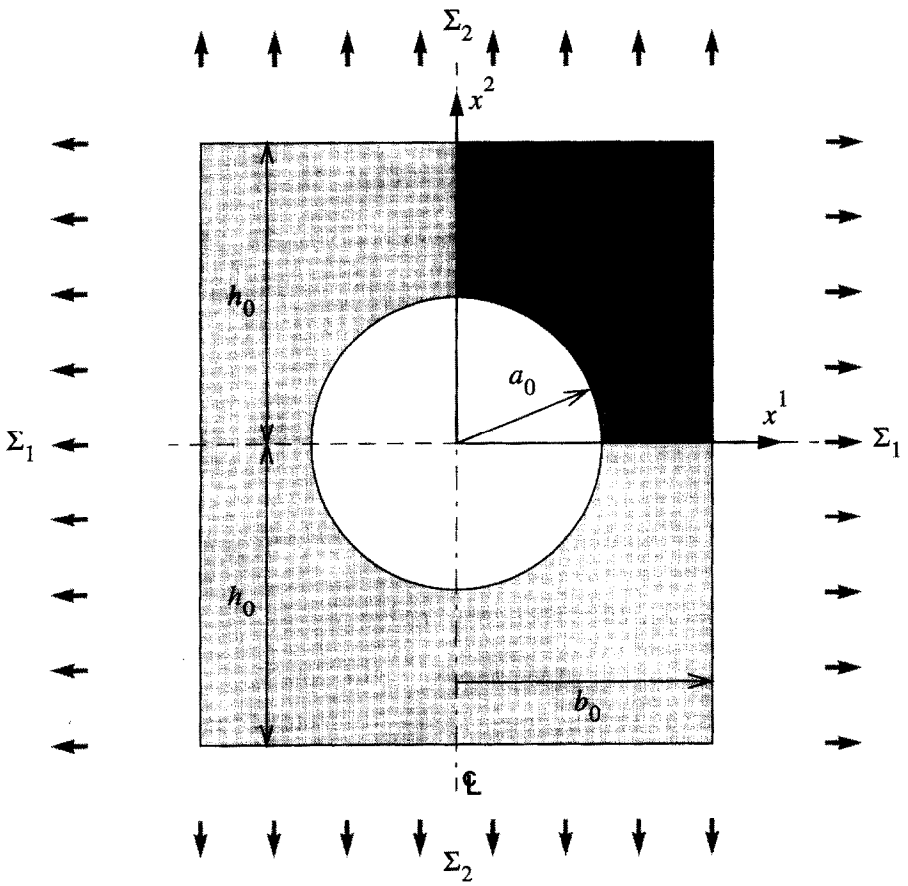

Fig. 1. Axisymmetric unit cell in the initial configuration. Only the shaded quadrant is analyzed.

$$E_1 = \ln(1+U_1/b_0), \quad E_2 = \ln(1+U_2/h_0).$$

The loading is strain controlled in such a way that the strain in the axial direction is prescribed at constant applied rate $\dot{E}_2$. The transverse strain-rate $\dot{E}_1$ is determined so that the stress ratio Σ_1/Σ_2 retains a constant, prescribed value. In that way, the remote stress triaxiality Σ_m/Σ_e is kept constant during the process. Here, Σ_e and Σ_m are the remote effective Mises stress and the remote mean stress, respectively, defined as

$$\Sigma_e = |\Sigma_2 - \Sigma_1|, \quad \Sigma_m = \tfrac{1}{3}(\Sigma_2 + 2\Sigma_1).$$

Furthermore, for the purpose of specifying the overall level of deformation, we use the macroscopic effective strain E_e

$$E_e = \tfrac{2}{3}|E_2 - E_1|.$$

This definition is motivated by the Mises effective strain-rate $\dot{\varepsilon}_e$, defined as $\dot{\varepsilon}_e = \sqrt{\frac{2}{3}\mathbf{D}' \cdot \mathbf{D}'}$ in terms of a deviatoric strain-rate tensor $\mathbf{D}'$. Substituting for $\mathbf{D}$ the macroscopic principle strain-rates $\dot{E}_1$ and $\dot{E}_2$, and assuming that the transverse strain-rate

$\dot{E}_1$ would remain constant during the deformation process, just like $\dot{E}_2$, the E_e would be equal to the accumulated Mises effective strain ε_e. Also, for future reference, we define an applied shear-rate $\dot{\Gamma}$ through

$$\dot{\Gamma} = \sqrt{\tfrac{3}{2}}|\dot{E}_2|.$$

This parameter corresponds to substituting the macroscopic strain-rates $\dot{E}_1$ and $\dot{E}_2$ into (6), for the unvoided material ($\dot{E}_1 = -\frac{1}{2}\dot{E}_2$).

The finite strain formulation of the problem is based on a Lagrangian description using convective coordinates x^i, with base vectors $\mathbf{g}_i$ in the undeformed configuration and base vectors $\mathbf{G}_i$ in the current configuration. Within the context of large plastic deformation problems for glassy polymers, the formulation and the method of solution is similar to that discussed in Wu and Van der Giessen (1996). That is, the governing equations are expressed in terms of the Lagrangian strain tensor $\boldsymbol{\eta}$ and the conjugate second Piola–Kirchhoff tensor $\boldsymbol{\tau}$. The solution is sought in a linear incremental way, based on the incremental virtual work expression

$$\Delta t \int_V (\dot{\sigma}^{ij}\delta D_{ij} + \sigma^{ij} v^k_{,i}\delta v_{k,j})\,\mathrm{d}V = \Delta t \int_S \dot{T}^i \delta v_i\,\mathrm{d}S, \tag{12}$$

for a time increment Δt, where V is the volume of the cell excluding the void, and S is the outer surface of cell. In writing the left-hand side of this expression we have made use of the identities

$$\dot{\eta}_{ij} = \mathbf{g}_i \cdot \dot{\boldsymbol{\eta}} \cdot \mathbf{g}_j \equiv D_{ij} = \mathbf{G}_i \cdot \mathbf{D} \cdot \mathbf{G}_j, \quad \tau^{ij} = \mathbf{g}^i \cdot \boldsymbol{\tau} \cdot \mathbf{g}^j \approx \sigma^{ij} = \mathbf{G}^i \cdot \boldsymbol{\sigma} \cdot \mathbf{G}^j,$$

neglecting the relative volume change $\det \mathbf{F} - 1$, in order to express the result in terms of the Cauchy stress $\boldsymbol{\sigma}$ and the rate of deformation $\mathbf{D}$. The v_i and T^i are the components of the velocity vector and traction vector, respectively, on the undeformed base vectors $\mathbf{g}_i$. The boundary conditions mentioned earlier are specified now as

$$\dot{v}_1 = 0, \quad T^2 = 0 \quad \text{along } x^1 = 0; \quad \dot{v}_1 = \dot{U}_1, \quad T^2 = 0 \quad \text{along } x^1 = b_0;$$

$$\dot{v}_2 = 0, \quad T^1 = 0 \quad \text{along } x^2 = 0; \quad \dot{v}_2 = \dot{U}_2, \quad T^1 = 0 \quad \text{along } x^2 = h_0.$$

The macroscopic applied stresses Σ_1 and Σ_2 are calculated at any instant from the tractions through

$$\Sigma_1 = \frac{b_0}{bh}\int_0^{h_0} T^1|_{x^1 = b_0}\,\mathrm{d}x^2, \quad \Sigma_2 = \frac{2}{b^2}\int_0^{b_0} (T^2 x^1)|_{x^2 = h_0}\,\mathrm{d}x^1.$$

The condition (12) is solved for by means of a finite element discretization using quadrilateral elements. Each quadrilateral element is built up of four constant strain triangular elements.

Provided that the various tensors are decomposed properly on the deformed base vectors $\mathbf{G}_i$, the constitutive equations in (1)–(11) can be immediately substituted into the left-hand side of (12). However, due to the highly nonlinear nature of the viscoplastic flow law (7), the time steps Δt need to be very small for numerical stability (Wu and Van der Giessen, 1994, 1995a). In order to improve the numerical stability, Wu and Van der Giessen (1996) have developed a rate tangent formulation of consti-

tutive equations in the spirit of the idea of Peirce *et al.* (1984). This formulation is based on a forward gradient estimate of the viscoplastic shear rate $\dot{\gamma}^{\mathrm{p}}$ at the instant $t+\theta\Delta t$. This finally leads to constitutive equations in the form

$$\overset{\nabla}{\boldsymbol{\sigma}} = \mathscr{L}\mathbf{D} + \dot{\boldsymbol{\sigma}}_{\mathrm{v}}, \tag{13}$$

where

$$\mathscr{L} = \mathscr{L}^{\mathrm{e}} - \mu \mathbf{M} \otimes \mathbf{M}, \quad \dot{\boldsymbol{\sigma}}_{\mathrm{v}} = -\frac{\dot{\gamma}^{\mathrm{p}}(t)}{1+\xi}\mathbf{M}, \quad \mu = \frac{1}{\sqrt{2}}\frac{\xi}{1+\xi}\frac{1}{g}, \quad \mathbf{M} = \frac{2G}{\sqrt{2}\tau}\bar{\boldsymbol{\sigma}}',$$

$$g = \frac{1}{\sqrt{2}}\left(2G + \frac{1}{2\tau^2}\bar{\boldsymbol{\sigma}}' \cdot \mathscr{R}'\bar{\boldsymbol{\sigma}}'\right), \quad \xi = g\theta\Delta t\frac{\partial \dot{\gamma}^{\mathrm{p}}}{\partial \tau}, \tag{14}$$

and G is the elastic shear modulus. The fourth-order tensor $\mathscr{R}'$ in (14) is the modulus tensor in the rate form

$$\overset{\nabla}{\mathbf{b}}' = \mathscr{R}'\mathbf{D}^{\mathrm{p}} \tag{15}$$

of the constitutive equations for the deviatoric back stress $\mathbf{b}'$. The $\mathscr{R}'$ is the deviatoric part of the modulus tensor, $\mathscr{R}$, for the full network model, which is approximated by the linear combination of three- and eight-chain moduli

$$\mathscr{R} = (1-\rho)\mathscr{R}^{3-\mathrm{ch}} + \rho\mathscr{R}^{8-\mathrm{ch}}. \tag{16}$$

The derivation of this rate form (15)–(16) from (9)–(11) involves a number of approximations, discussed in (Wu and Van der Giessen, 1996). One of the most notable approximations is that the value of the plastic principal stretches are instantaneously determined from the current total stretches of the continuum. Thus, the elastic stretches are neglected relative to the total ones. Note that, eventually, the rate tangent modulus tensor $\mathscr{L}$ to be substituted into (12) is dependent on the viscoplastic properties through g and on the time increment Δt through ξ. The viscoplastic stress increments $\dot{\boldsymbol{\sigma}}_{\mathrm{v}}\Delta t$ from (13) are naturally combined with the nodal traction-increment vector in the right-hand side of (12). An equilibrium correction term is added to the incremental virtual work condition (12) to avoid drifting of the solution from the true equilibrium path in the course of the incremental procedure.

The update of the state at the end of each incremental step can be done consistently with the linear incremental form of the constitutive equations (13). However, it has been shown (Wu and Van der Giessen, 1996) to be convenient to compute the current back stress tensor $\mathbf{b}$ immediately from the updated state of deformation by means of (9)–(11). The implementation also incorporates an adaptive time stepping scheme, which is similar to that described in some detail in Wu and Van der Giessen (1994). It involves a simple, heuristic yet efficient method that sets the time step Δt for each increment such that a number of criteria are satisfied. In the present computations, two constitutive criteria were used, which ensured that the shear strength drop according to (8) during an increment Δt does not exceed 1% of the initial shear strength s_0 and that the plastic shear strain increment $\dot{\gamma}^{\mathrm{p}}\Delta t$ remains smaller than 1%.

4. CELL MODEL RESULTS

A full parametric study for the material class under consideration does not seem feasible nor necessary at this stage to gain an understanding of the deformation processes around voids in such materials. Therefore, we restrict the presentation to the material parameters that are key to the mechanisms. The reference set of material parameters is chosen to be representative for a typical amorphous glassy polymer such as polycarbonate (PC) at room temperature, and is similar to that used in previous work (Wu and Van der Giessen, 1994, 1995a). That is, $\nu = 0.3$, $s_{ss}/s_0 = 0.79$, $As_0/T = 79.2$, $h/s_0 = 5.15$, $\alpha = 0.08$, $N = 6.3$ and $C^R/s_0 = 0.059$. As discussed also by Wu and Van der Giessen (1994), the elastic modulus E is chosen not to be equal to the initial Young's modulus, since amorphous glassy polymers generally exhibit a small strain viscoelastic effect resulting in a nonlinear stress–strain response prior to yielding. Therefore, E is chosen to match the ratio between yield stress and yield stain in uniaxial tension, which leads to a typical value of $E/s_0 = 9.38$. Some variations will be considered in the strain softening characteristic determined by h/s_0. In all cases, the applied strain-rate $\dot{E}_2$ is specified relative to the reference shear-rate $\dot{\gamma}_0$ as $\dot{E}_2/\dot{\gamma}_0 = 0.5 \times 10^{-17}$. For the purpose of reference, the true stress–logarithmic strain response for the unvoided material in uniaxial tension at the same strain-rate $\dot{\varepsilon}$ is shown in Fig. 2 for the parameter combinations that will be used.

We present results for computations using a unit cell with $h_0 = b_0$, thus representing a more or less uniformly voiding material. Attention is confined to two initial void volume fractions. The largest value of $f_0 = 0.083$ corresponding to $a_0/b_0 = 0.5$ is motivated by the volume percentage of rubber particles that is typically used in polymer–rubber blends. Rubber contents of 30% are quite common, but micrographs indicate that not all rubber particles actually cavitate [see, e.g. Bucknall (1977)], and

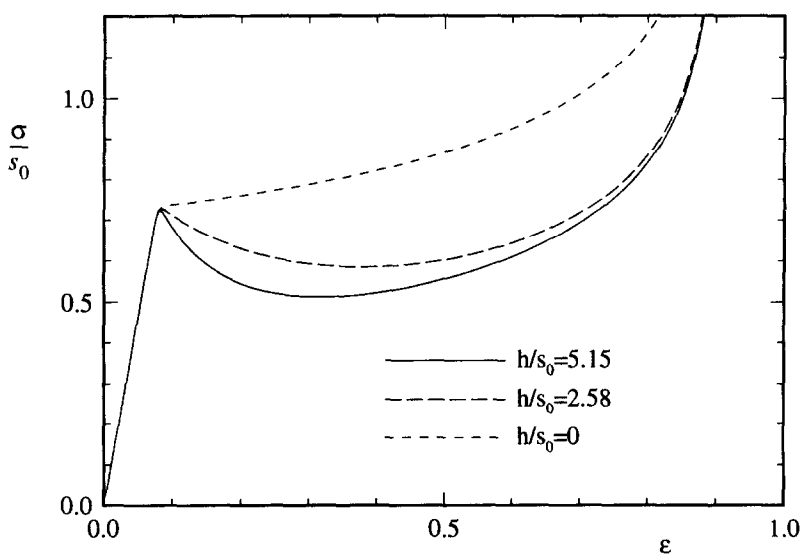

Fig. 2. True stress σ versus logarithmic strain ε curves in uniaxial tension for the various values of h/s_0 used in this paper.

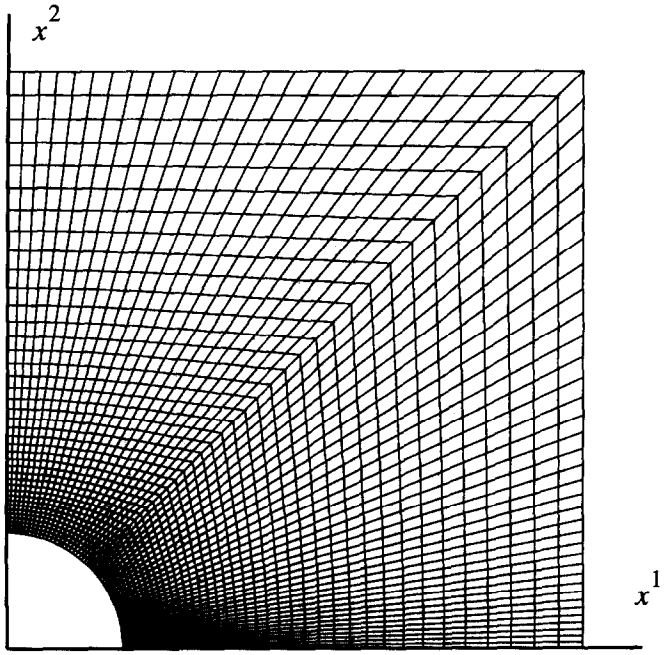

Fig. 3. Mesh used for the cases with $a_0/b_0 = 0.2$. The mesh used for $a_0/b_0 = 0.5$ has a similarly fine mesh around the void.

therefore we have chosen the initial void volume fraction to be around a factor 3 lower. To get some insight into the effect of interactions between voids at this void volume fraction, a lower void volume fraction of $f_0 = 0.0053$ is considered as well, and this corresponds to taking $a_0/b_0 = 0.2$. In order to pick up the localized deformations that develop for the materials under consideration, a relatively fine mesh is needed around the void, especially near the equator. Figure 3 gives an example of the undeformed mesh used for voids with $a_0/b_0 = 0.2$.

Results are presented for a range of remote stress triaxialities between $\Sigma_m/\Sigma_e = 1/3$, corresponding to uniaxial tension ($\Sigma_1 = 0$), and $\Sigma_m/\Sigma_e = 3$, which is commonly viewed as pertaining to the stress state ahead of a crack tip. Figure 4 shows the overall response as a function of the overall effective strain E_e for a material with the above reference properties and with an initial void size $a_0/b_0 = 0.5$ under different stress triaxialities. Results are given for the macroscopic effective stress Σ_e response, and for the evolution of the void volume fraction f and the area strain $\ln(b_0/b)^2$. A global view at these results indicate that there is quite a significant difference in the nature of the response under low triaxiality, $\Sigma_m/\Sigma_e = 1/3$, as compared to that under the highest triaxiality. In order to get a better understanding of the origins of these differences, Figs 5–7 present snapshots of the instantaneous deformation modes in terms of distributions of the current values of the plastic shear rate $\dot{\gamma}^p$.

Figure 5 shows the plastic shear rate distributions at three instants during uniaxial straining, plotted on a scale from 0 to 6 times the applied shear rate $\dot{\Gamma}$. Figure 5(a) shows the occurrence of substantial plasticity even though the strain is below the

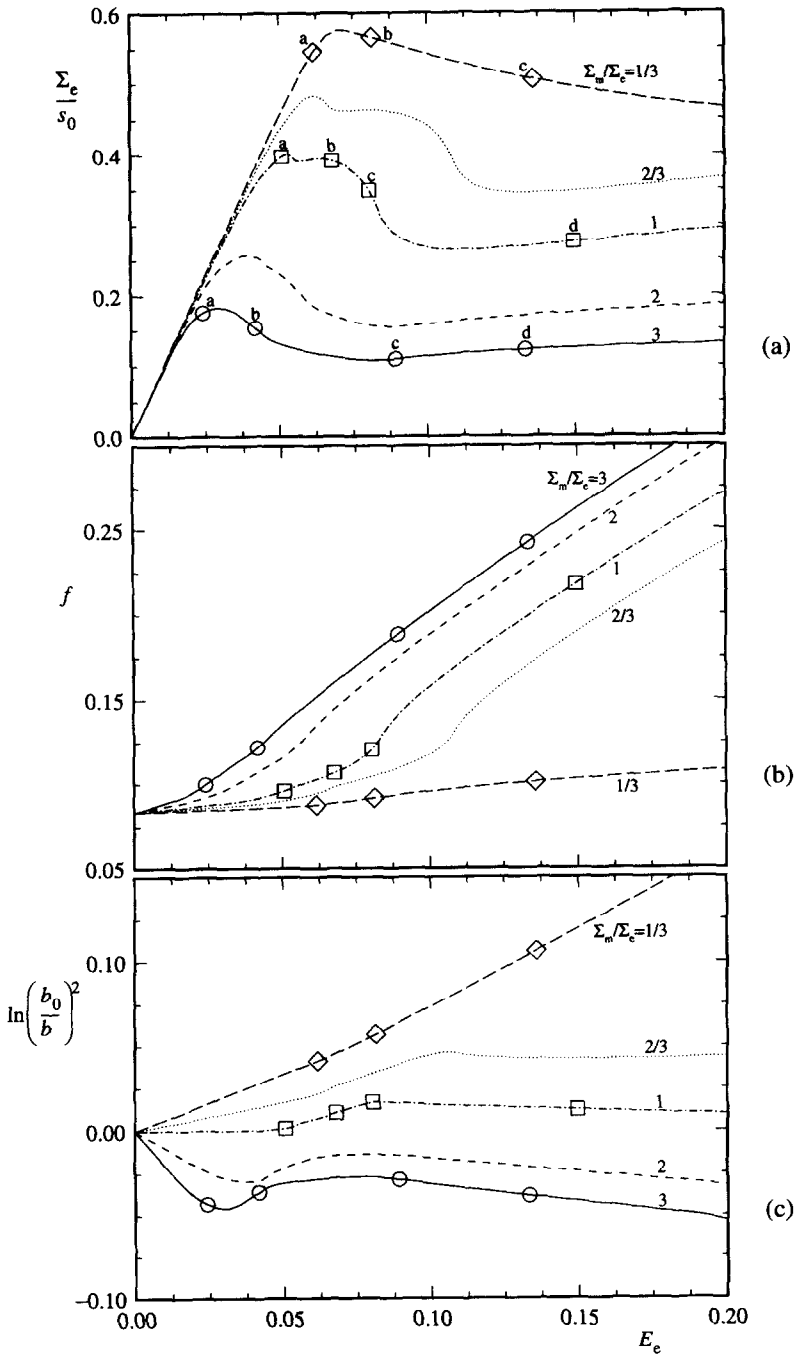

Fig. 4. Response to different remote stress triaxialities Σ_m/Σ_e for material with $h/s_0 = 5.15$ and with the initial void specified by $a_0/b_0 = 0.5$ ($f_0 = 0.083$). (a) Macroscopic effective stress response; (b) evolution of the void volume fraction f; (c) evolution of the area strain. The enumerated symbols refer to the plots shown in subsequent figures: Fig. 5: ◇; Fig. 6: □; Fig. 7: ○.

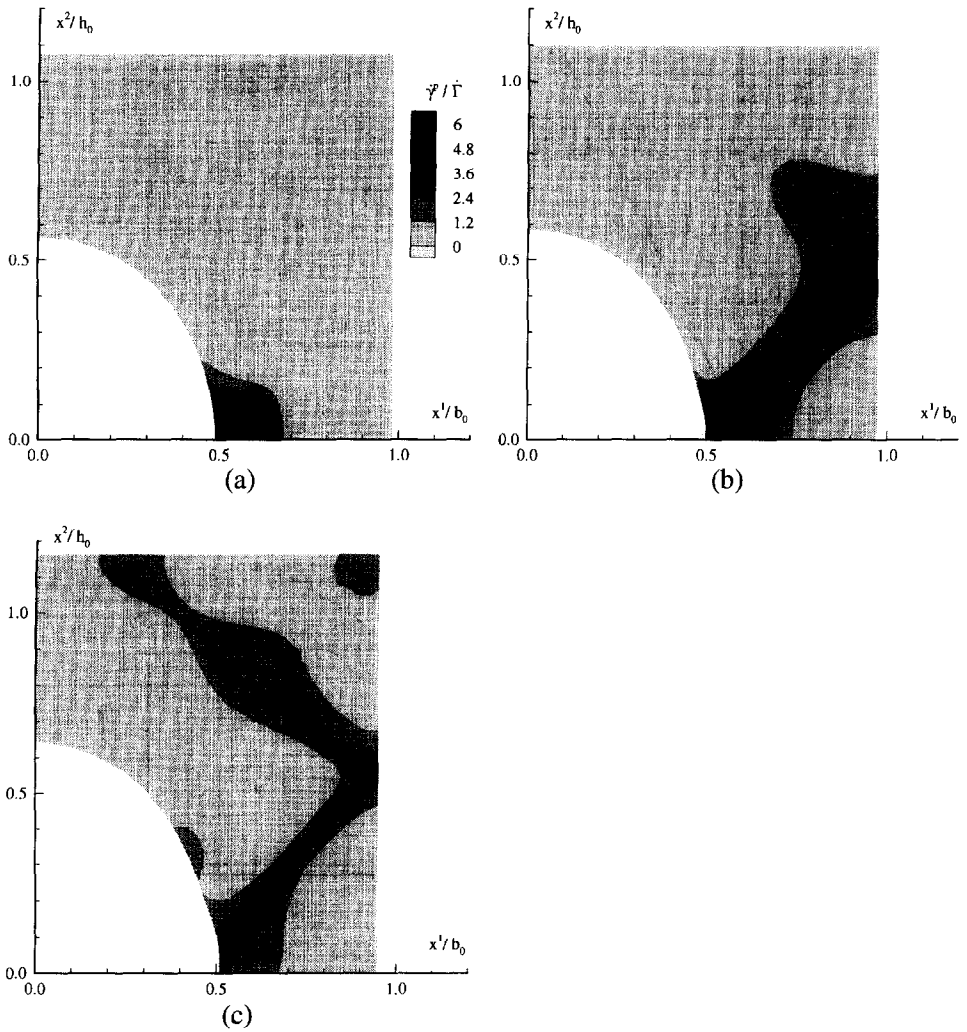

Fig. 5. Distribution of plastic shear rate corresponding to the case in Fig. 4 for uniaxial tension, $\Sigma_m/\Sigma_e = 1/3$. (a) $E_e = 0.062$; (b) $E_e = 0.082$; (c) $E_e = 0.139$.

strain at which the macroscopic stress–strain response attains a "macroscopic yield" point (at $E_e = 0.07$). It is noted that for any stress triaxiality with $\Sigma_2 > 0$, Goodier's (1933) solution for a void in an elastic infinite medium proves that the maximum value of the effective shear stress $\tau = \sqrt{\frac{2}{2}\boldsymbol{\sigma}\cdot\boldsymbol{\sigma}}$ [cf. (5)] occurs at the equator of the void, $x^1 = a_0$. Plasticity is therefore initiated at the equator. Since local yield is immediately followed by local strain softening, the plastic zone will rapidly expand. Soon after, a band of plastic shear activity emerges from the void equator [see Fig. 5(b)] as the macroscopic Mises stress attains a maximum. Initially, this "shear band" is oriented at 45° relative to the x^2-axis. During continued deformation, further localization of deformation occurs in the band. As strain hardening eventually occurs inside the band, adjacent material becomes more prone to plasticity and strain soften-

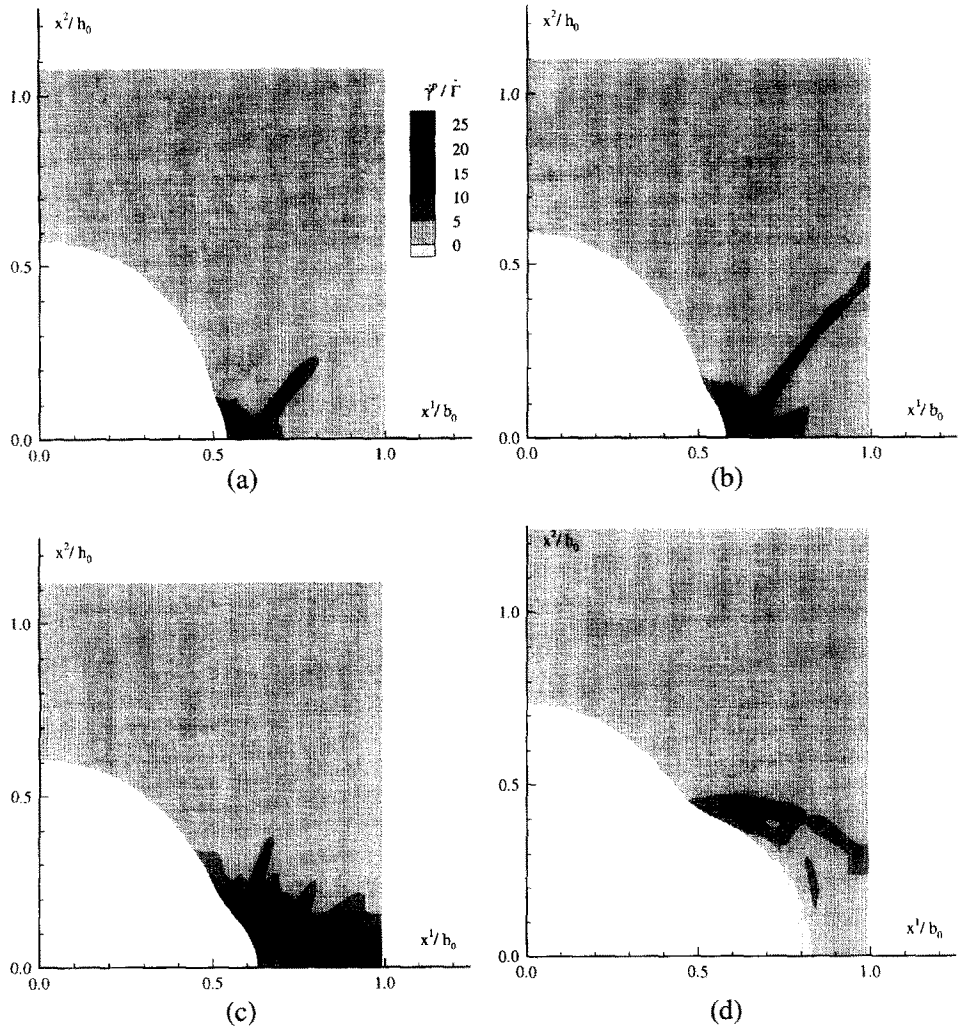

Fig. 6. Distribution of plastic shear rate corresponding to the case in Fig. 4 for $\Sigma_m/\Sigma_e = 1$. (a) $E_e = 0.051$; (b) $E_e = 0.068$; (c) $E_e = 0.080$; (d) $E_e = 0.149$.

ing, so that the band of localized plasticity propagates as a whole in the loading direction, as is seen in Fig. 5(c). As a consequence, the void grows into an oblate spheroidal-like shape, with a smooth overall contraction b/b_0 and with a slow monotonic growth of the void volume fraction f [see Fig. 4(b) and (c)].

At a remote stress triaxiality of $\Sigma_m/\Sigma_e = 1$, plasticity near the equator of the void also leads to an inclined 45° shear band from the equator [see Fig. 6(a)]. However, shortly after the shear band has propagated through the ligament, i.e. beyond macroscopic yield, a second band of localized plasticity emerges in the neighbourhood of the equator but at an orientation of about $-30°$ [see Fig. 6(b)]. With ongoing deformation, plastic flow rather massively localizes in this second band [see Fig. 6(c)], which leads to a rapid substantial drop in the overall stress (see Fig. 4a). While this

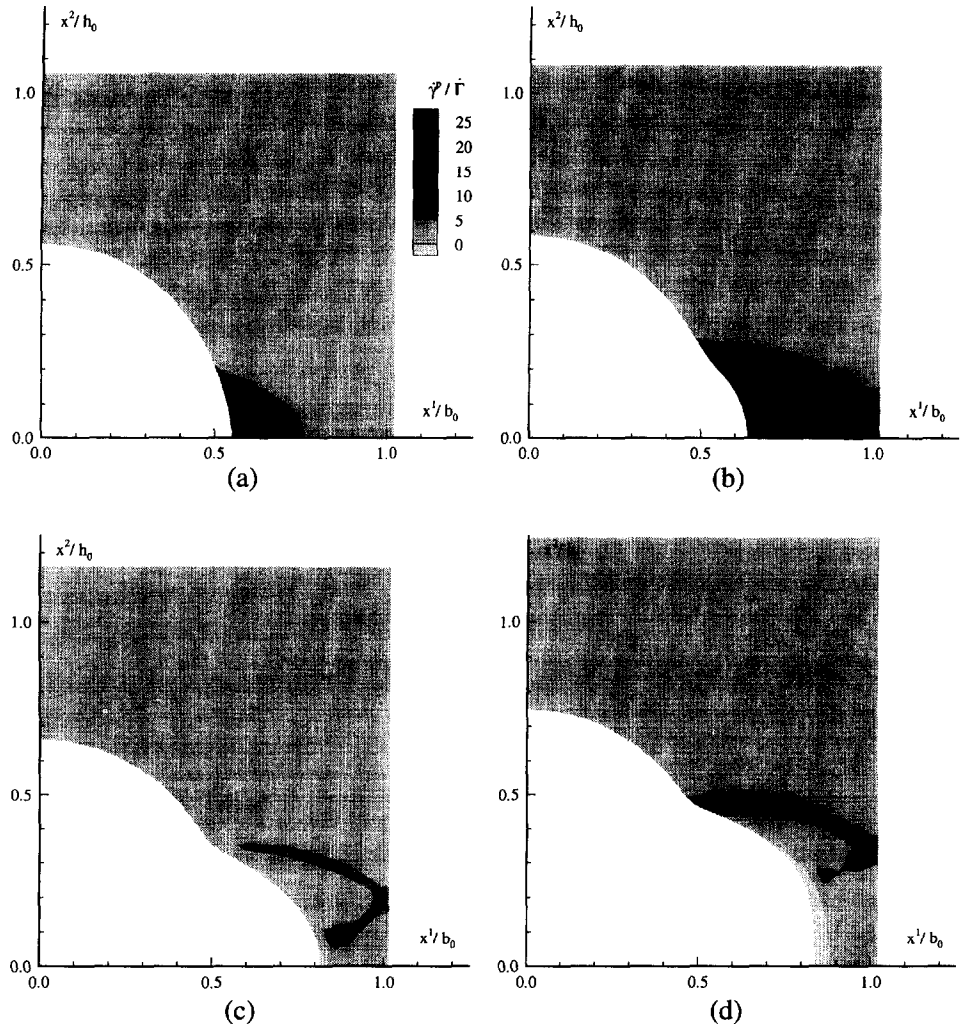

Fig. 7. Distribution of plastic shear rate corresponding to the case in Fig. 4 for $\Sigma_m/\Sigma_e = 3$. (a) $E_e = 0.024$; (b) $E_e = 0.041$; (c) $E_e = 0.089$; (d) $E_e = 0.133$.

occurs, the void growth rate is seen from Fig. 4(b) to be accelerated due to rather local growth of the void in the x^1-direction (bulging). It is noted that Fig. 6(c) indicates that during the overall softening there is a competition between a number of short shear band-like zones. With continued deformation, the initial shear bands lock-up due to strain hardening and the second, somewhat curved, shear band survives and propagates upwards. Growth of the voids now occurs mainly by progressive bulging caused by the propagating shear band, as is clearly visible in Fig. 6(d).

At the highest stress triaxiality considered here, $\Sigma_m/\Sigma_e = 3$, we see that the tendency for formation of an inclined shear band is completely absent. Rather, Fig. 7(a) shows a declining shear band right from the early stages of deformation. After macroscopic yield [see Fig. 4(a)], plasticity further localizes inside this band [see Fig. 7(b)]. Void

expansion then occurs primarily by outward wedging of the material below the shear band and lateral contraction of the remaining material, contrary to the lateral expansion prior to macroscopic yield. Further deformation leads to propagation of the shear band [see Fig. 7(c) and (d)] at almost constant applied stress [see Fig. 4(a)].

It is pertinent at this point to note that, due to the viscoplastic nature of the material response, the thickness of the shear bands found here is set by the problem under consideration [see also Wu and Van der Giessen (1996)]. Hence, there is no pathological mesh dependence, but the mesh should be fine enough to be able to resolve the shear bands. A slight dependence on the mesh orientation does remain, however, as shear bands in the elements used here occur preferentially along element diagonals. The initial mesh size and orientation used here have been tuned to have the proper orientation and to be sufficiently fine to capture the main characteristics.

It is seen from Figs 5–7 that the shear bands that govern the behaviour beyond macroscopic yield extend throughout the ligament between voids. This raises a question concerning the interaction between voids in these cases of an initial void volume fraction $f_0 = 0.083$. In order to get some feeling for this, the cases have been repeated with a smaller initial void size, specified by $a_0/b_0 = 0.2$ corresponding to $f_0 = 0.0053$. The overall responses to the same remote stress triaxialities as before, are shown in Fig. 8. Comparing the results with the corresponding ones for the larger void size in Fig. 4, it appears that the responses as a function of triaxiality fall into two categories: those for $\Sigma_m/\Sigma_e \leqslant 1$ approximately are similar in phenomenology to the uniaxial stress result in Fig. 4, whereas the responses for $\Sigma_m/\Sigma_e \geqslant 2$ are similar to the high-triaxiality results in Fig. 4. This dichotomy is particularly evident in the evolution of f and of the area strain $\ln (b_0/b^2)$. Drawing on the observations made above relative to the deformation modes corresponding to Fig. 4, it is expected that the first category of responses in Fig. 8 are dominated by inclined shear bands (at around 45°), while the second is controlled by the declined shear bands at $-30°$. This is confirmed by the distributions of the instantaneous plastic shear rate shown in Fig. 9 for uniaxial tension and in Fig. 10 for high triaxiality $\Sigma_m/\Sigma_e = 3$. Furthermore, these plastic shear activity plots indicate that for this relatively small initial void size, the inclined shear band propagates only partially into the ligament (see Fig. 9). There seems to be still some interaction between voids, but it is rather weak throughout the process. Under high triaxiality, in Fig. 10, we observe that the declined shear bands are confined initially to the immediate vicinity of the void, but that propagation occurs both in the maximum principal stress direction as well as in the lateral direction. In the later stages, shown, e.g. in Fig. 10(b), the shear band spans the entire ligament, so that void–void interaction is an important factor in the void evolution.

All results presented, show that void growth in glassy polymers involves one of two types of shear bands. The shear bands inclined at 45° is favoured by low triaxialities and small voids, whereas the others are favoured by high triaxiality and large voids. The latter appears to have an orientation of around $-30°$ with the normal to the macroscopic principal stress; but in fact, at their point of initiation at the void surface, they are oriented at $-45°$ to the radial direction [see Figs 7(a) and 10(a)]. Even though we are dealing here with axisymmetric problems, the latter type of shear bands are reminiscent of the slip line fields at planar, rounded notches. The formation of each of the two shear band types give distinct appearances in the area strain, $\ln (b_0/b)^2$,

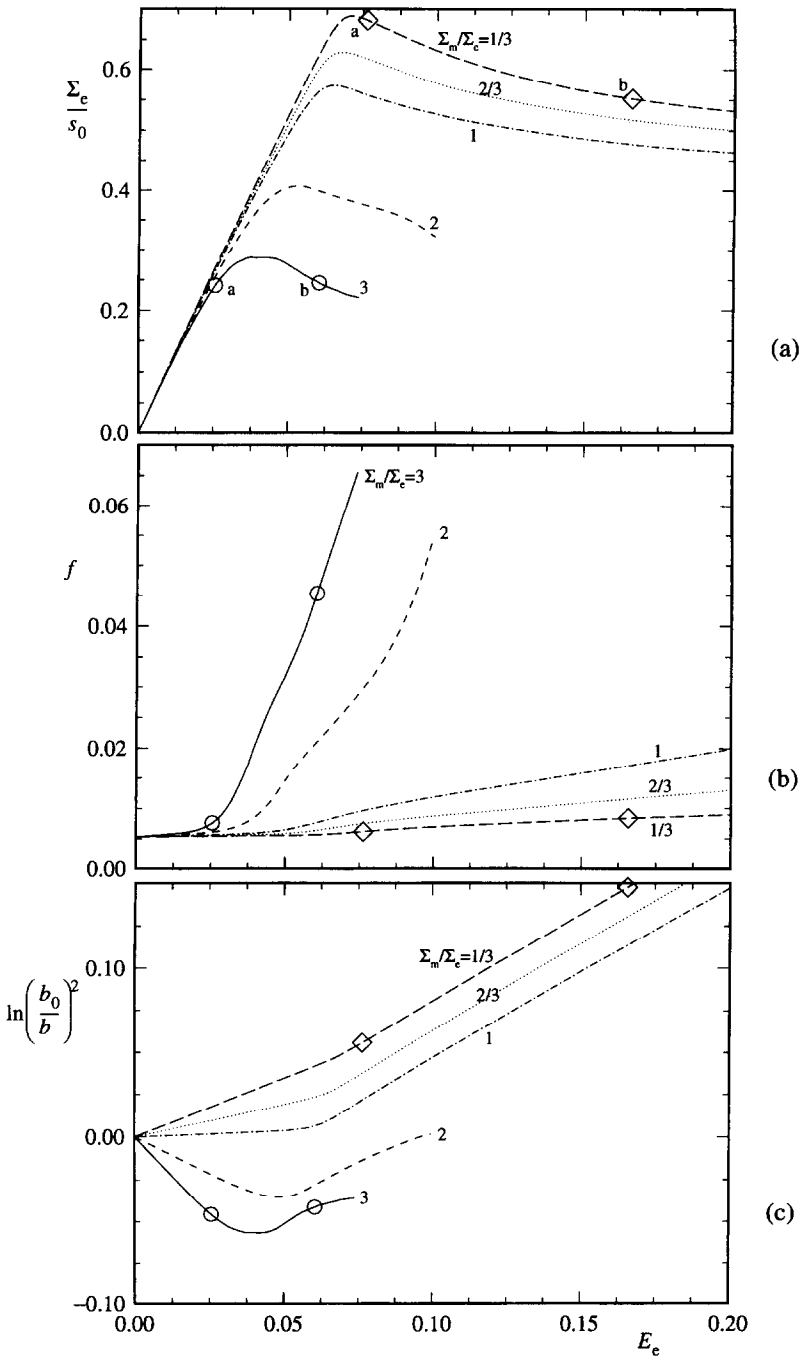

Fig. 8. Response to different remote stress triaxialities Σ_m/Σ_e for material with $h/s_0 = 5.15$ and with the smaller initial void, specified by $a_0/b_0 = 0.2$ ($f_0 = 0.0053$). (a) Macroscopic effective stress response; (b) evolution of the void volume fraction f; (c) evolution of the area strain. The enumerated symbols refer to the plots shown in subsequent figures: Fig. 9: ◇; Fig. 10: ○.

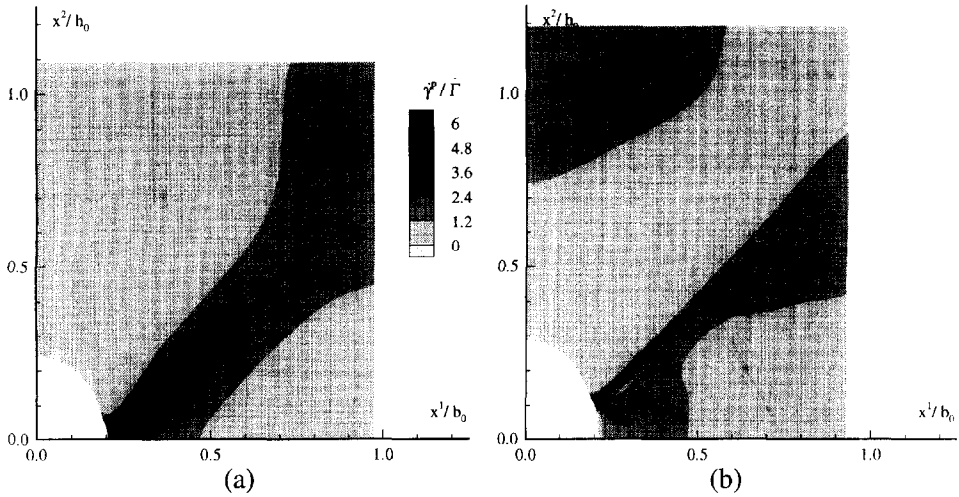

Fig. 9. Distribution of plastic shear rate corresponding to the case in Fig. 8 for $\Sigma_m/\Sigma_e = 1/3$.

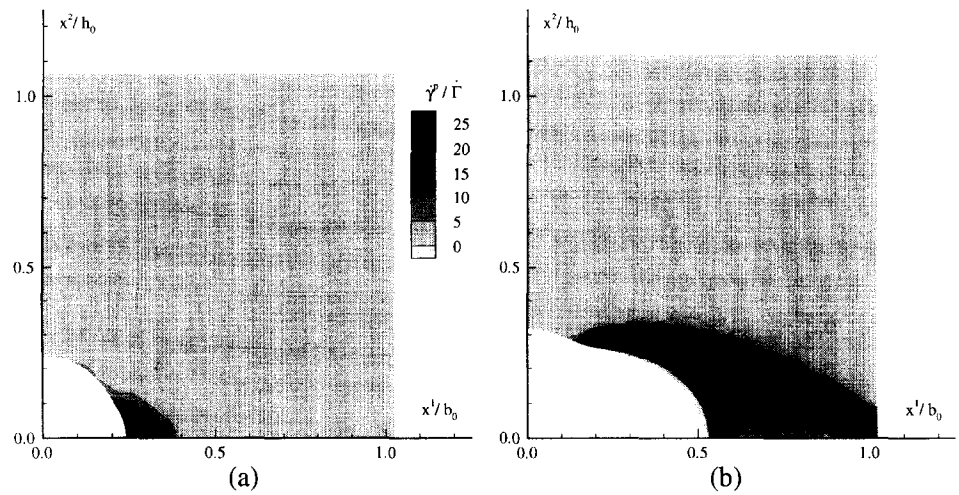

Fig. 10. Distribution of plastic shear rate corresponding to the case in Fig. 8 for $\Sigma_m/\Sigma_e = 3$.

evolution shown in Figs 4(c) and 8(c). A 45° shear band gives rise to a kink due to the associated increased lateral contraction of the cell, whereas a $-30°$ shear band gives a sign change in the rate of change of the area strain, i.e. the initial lateral expansion in those cases changes to contraction upon initiation of the declined shear band.

The initiation and propagation of shear bands in the type of materials considered here is primarily controlled by the rate of softening upon yield. In the formulation given in Section 2, there is a slight effect of C^R and N on the rate of softening, but this is primarily determined by h/s_0 [cf. (8)]. The effect of a much smaller softening rate, $h/s_0 = 2.58$, and essentially no softening, $h/s_0 = 0$, on the intrinsic behaviour of

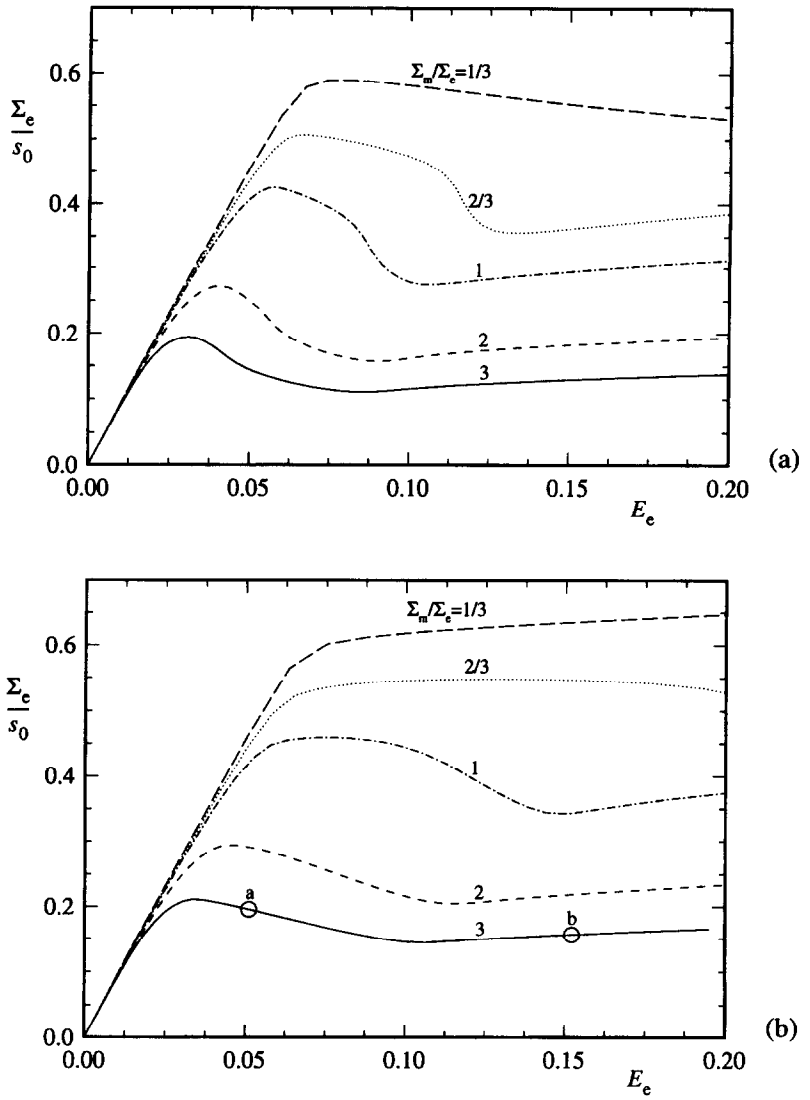

Fig. 11. Effect of h/s_0 on the macroscopic stress–strain response for material with $a_0/b_0 = 0.5$ ($f_0 = 0.083$): (a) $h/s_0 = 2.58$; (b) $h/s_0 = 0$.

the matrix has been shown in Fig. 2, and the effect on the porous material behaviour is shown in Fig. 11. Even though reducing h will reduce the tendency to shear banding, macroscopic softening still takes place due to void growth (Fig. 11), especially under higher triaxialities. But, the strain at which the macroscopic stress drop takes place is delayed when the softening rate is reduced. Figure 12, for $\Sigma_m/\Sigma_e = 3$, shows that the plastic flow around the void in the absence of intrinsic softening, $h = 0$, is much more diffuse than in the presence of softening, as was shown in Fig. 7.

All the results presented, show that the growth of the void after macroscopic yield

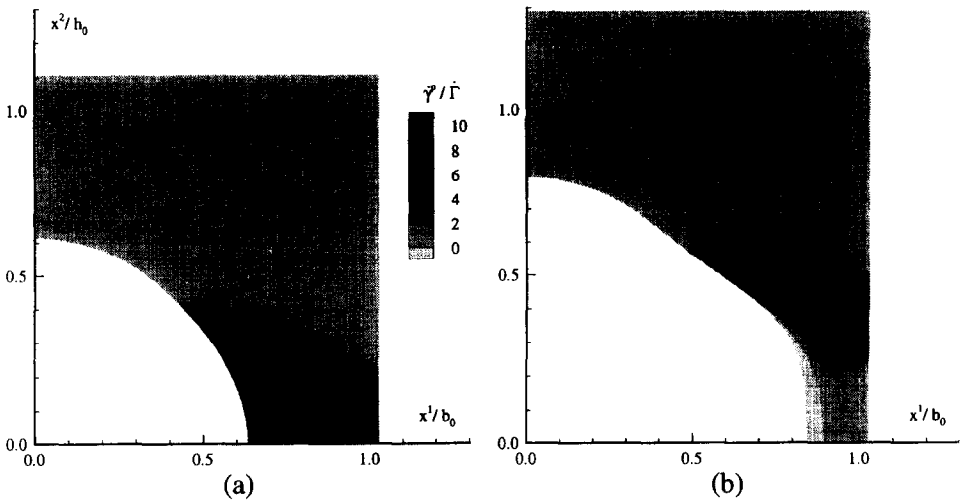

Fig. 12. Distribution of plastic shear rate corresponding to the case in Fig. 11(b) ($h/s_0 = 0$) for $\Sigma_m/\Sigma_e = 3$.

occurs by propagation of the region of instantaneous plastic flow in the tensile direction. This gives rise to "drawing" of the ligament between voids, similar to the drawing of tensile bars of these materials due to neck propagation. It is interesting to note that in materials that exhibit a typical metal-like strain hardening plasticity, necking of the ligament also occurs. However, then necking takes place progressively due to the falling strain hardening response, and this leads to coalescence of the voids by collapse of the ligament (Koplik and Needleman, 1988).

5. MODIFIED GURSON MODEL

5.1. *Formulation*

Gurson's (1977) derivation of an approximate yield function for a porous rigid-plastic metal has formed the basis for many recent investigations into ductile fracture. Some improvements of the original Gurson yield surface have been suggested by Tvergaard (1981, 1982), and several subsequent modifications have been proposed to incorporate effects of void nucleation and void coalescence. In view of the nature of the constitutive model considered here, we explicitly mention the kinematic hardening version introduced by Mear and Hutchinson (1985) as well as the corresponding viscoplastic formulation of Becker and Needleman (1986). It is in the spirit of these papers that we formulate a Gurson-type model for porous glassy polymers in the following manner.

Following Becker and Needleman (1986), we start out by introducing a potential Φ as

$$\Phi = \frac{1}{2}\frac{\bar{\boldsymbol{\sigma}}' \cdot \bar{\boldsymbol{\sigma}}'}{\tau^2} + 2q_1 f \cosh\left(\frac{\sqrt{3}}{2} q_2 \frac{\sigma_m}{\tau}\right) - [1 + (q_1 f)^2] = 0, \tag{17}$$

where f is the current void volume fraction, and q_1 and q_2 are parameters introduced by Tvergaard (1981, 1982). Note that the potential is formulated here in terms of the effective shear stress rather than in terms of the effective Mises stress. Also note that, contrary to the kinematic hardening formulation of Mear and Hutchinson (1985), the mean stress dependence is expressed through the Cauchy mean stress $\sigma_m = \frac{1}{3}\mathrm{tr}\,\boldsymbol{\sigma}$, since the hydrostatic part of the back stress in the present model is left indeterminate. Based on this potential, Becker and Needleman (1986) express the plastic strain-rate through the normality rule

$$\mathbf{D}^p = \dot{\Lambda}\frac{\partial \Phi}{\partial \bar{\boldsymbol{\sigma}}}, \tag{18}$$

where $\dot{\Lambda}$ is obtained from the condition that the plastic work rate in the porous material per unit volume, $\dot{\boldsymbol{\sigma}} \cdot \mathbf{D}^p$ be equal to the dissipation in the matrix material, i.e.

$$\bar{\boldsymbol{\sigma}} \cdot \mathbf{D}^p = (1-f)\sqrt{2}\tau\dot{\gamma}^p,$$

with $\dot{\gamma}^p$ being given as a function of τ through (7). From (18) it then follows that

$$\dot{\Lambda} = (1-f)\sqrt{2}\tau\dot{\gamma}^p \left(\bar{\boldsymbol{\sigma}} \cdot \frac{\partial \Phi}{\partial \bar{\boldsymbol{\sigma}}}\right)^{-1}.$$

It is to be noted that in this formulation for a porous glassy polymer, the driving stress τ is no longer defined by (5) as for the unvoided matrix material, but is to be determined from the condition $\Phi = 0$ according to (17). For $f = 0$, τ from (17) reduces to (5), and the flow rule (18) reduces to (4).

Apart from the parameters q_1 and q_2, the potential Φ according to (17) is directly based on Gurson's (1977) spherical model of a void in an infinite, incompressible, rigid-plastic material. With a view on applications in ductile metals, where the elastic strains remain much smaller than the plastic strains, effects of elasticity on overall yield of the porous material are neglected in Gurson's analysis. Also, the elastic compressibility of the porous matrix, i.e. due to elastic void growth, is commonly neglected in applications to ductile metals [see, e.g. Tvergaard (1981, 1982) and Koplik and Needleman (1988)]. However, for the present application to amorphous polymers, with yield strains of the order of 5%, elastic effects can be quite significant, as will be demonstrated in the next section. Numerical studies have indicated that the elastic effects are most dominant under highly triaxial stress states. Therefore, we have carried out an approximate analysis of an elastic–viscoplastic hollow sphere with an outer radius equal to the initial half-spacing b_0 between voids in Fig. 1 and an initial inner radius of a_0 subjected to external hydrostatic tension. The analysis (see Appendix) suggests a modification of the mean stress dependent term in the potential, and the modified potential then becomes

$$\Phi = \frac{1}{2}\frac{\bar{\boldsymbol{\sigma}}' \cdot \bar{\boldsymbol{\sigma}}'}{\tau^2} + 2q_1 f \cosh\left(e \ln\left[1 + \frac{1}{e}\frac{\sqrt{3}}{2}\frac{\sigma_m}{\tau}\right]\right) - [1 + (q_1 f)^2] = 0. \tag{19}$$

The correction for elasticity is controlled by the parameter e, defined by

$$e = \ln(\tau/E),$$

which depends on the yield strain in the matrix material. It is readily verified that when elasticity is negligible, i.e. $e \to -\infty$, the potential (19) reduces asymptotically to the Gurson-type expression (17).

The change of the void volume fraction f due to growth of the voids during a deformation process is governed by the evolution relation

$$\dot{f} = (1-f)\,\mathrm{tr}\,\mathbf{D}^{\mathrm{p}} + \dot{f}^{\mathrm{e}}, \tag{20}$$

expressing conservation of mass. Here, the elastic dilatation f^{e} is estimated from the Lamé solution for an elastic thick-walled sphere under hydrostatic stressing (as considered in the Appendix, but for a compressible elastic solid). In rate form, the result reads

$$\dot{f}^{\mathrm{e}} = f_0 \frac{3\dot{\sigma}_{\mathrm{m}}}{4G} \tag{21}$$

with $G = E/2(1+\nu)$ being the elastic shear modulus.

The void volume fraction has a small effect on the elastic properties of the porous material. Thus, the overall elastic moduli are taken according to (3) but with the Young's modulus and Poisson's ratio replaced with parameters E^* and ν^*, respectively, which depend on the current void volume fraction f. Following Jeong and Pan (1995), we use the following self-consistent estimates from Tandon and Weng (1988)

$$E^* = \frac{2E(7-5\nu)(1-f)}{2(7-5\nu)+(1+\nu)(13-15\nu)f}, \tag{22}$$

$$\nu^* = \frac{2\nu(7-5\nu)+(1+\nu)(3-5\nu)f}{2(7-5\nu)+(1+\nu)(13-15\nu)f}. \tag{23}$$

5.2. *Comparison with cell model results*

In order to check the adequacy of the above Gurson-type model for porous glassy polymers, we confront its predictions with the cell model results. This is done by identifying the macroscopic stresses Σ_1, Σ_2 and macroscopic strain rates E_1 and E_2 in the cell model with the corresponding components of stress $\boldsymbol{\sigma}$ and strain-rate $\mathbf{D}$ entering in the Gurson-type constitutive equations (17)–(20) (Koplik and Needleman, 1988). Prescribing the Cartesian strain-rate coordinates D_{22} and requiring a constant ratio σ_{11}/σ_{22}, similar to the boundary conditions in the cell model analyses (Section 3), the Gurson constitutive equations can be readily integrated in time.

Since Gurson (1977) derived his original yield function that underlies (17) for a J_2, non-hardening material, we first consider cases for a material without any softening ($h = 0$) and without any orientational hardening ($C^{\mathrm{R}} = 0$). For the same two initial void volume fractions as studied in the previous section, $f_0 = 0.0053$ and 0.083, Fig. 13 shows the yield potential $\Phi = 0$ according to (19) for the same fixed axial strain-rate D_{22}, plotted in the macroscopic stress space $\Sigma_{\mathrm{e}} - \Sigma_{\mathrm{m}}$. Also shown are some macroscopic yield points according to cell analyses with the same matrix material and macroscopic strain-rate $\dot{E}_2$ for some triaxialities values ranging from pure shear ($\Sigma_{\mathrm{m}} = 0$) to pure hydrostatic loading ($\Sigma_{\mathrm{e}} = 0$). For a proper comparison, Fig. 13(a) first shows results

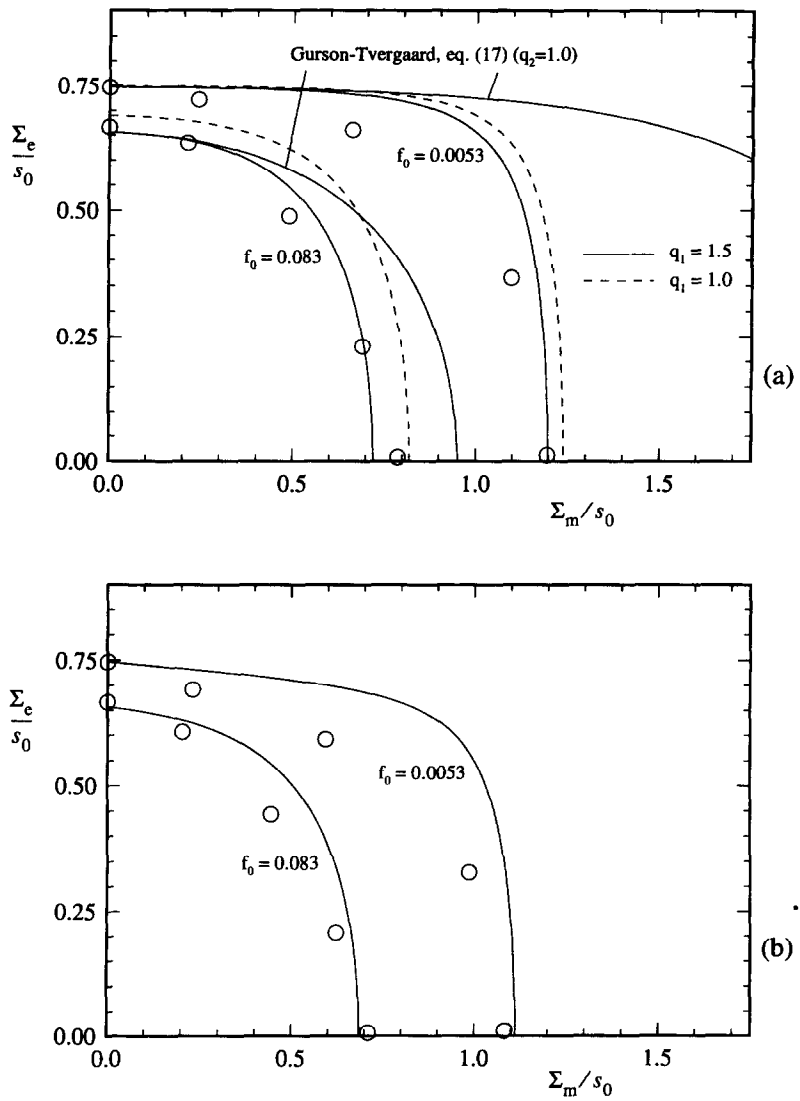

Fig. 13. Yield surface predicted by the modified potential (19) for a material without softening and hardening, $h = C^R = 0$. The symbols ○ indicate macroscopic yield stresses at different triaxialities according to the cell analyses. (a) No pressure dependence of yielding, $\alpha = 0$, as in Fig. 14; (b) $\alpha = 0.08$, as elsewhere.

where the pressure dependence of viscoplastic flow is discarded, $\alpha = 0$. First of all, it is seen that for purely hydrostatic stress states, the predictions of the modified potential (19) ($q_1 = 1$) are in excellent agreement with the cell analyses for both void fractions. At lower triaxialities, however, the potential (19) overestimates the yield stresses. An important reason for this is that the effects of the hydrostatic and deviatoric stresses in (19) are decoupled, with the hydrostatic term being based on spherically symmetric

fields. In the cell analyses however, plasticity tends to concentrate into the ligament [Fig. 12(a) gives an indication of this]. A best fit of the cell model results over the entire triaxiality range is obtained by taking a value $q_1 = 1.5$ in (19). This value is the same as originally suggested by Tvergaard (1981, 1982), while the second Tvergaard parameter q_2 in (17) has been abandoned. For comparison, Fig. 13(a) also shows the original Gurson–Tvergaard potential with the same value of $q_1 = 1.5$ (and $q_2 = 0$), and it is seen that the present modifications achieve a considerable improvement over the original criterion in the high triaxiality regime (see also Appendix).

Figure 13(b) provides similar results, but now for a matrix material that does exhibit pressure dependent flow, i.e. $\alpha = 0.08$ as in the other studies in this paper. As discussed also by Jeong and Pan (1995) in the context of a time independent rigid-plastic material model, the yield stresses are increasingly reduced relative to those for $\alpha = 0$ with increasing value of $\Sigma_m/\Sigma_e > 0$. The modified potential (19) is seen to incorporate this pressure sensitivity fairly well.

In addition to giving an adequate estimate of the yield point, one may also want the macroscopic constitutive theory to provide an approximate description of the entire overall stress–strain response and the associated void evolution. Figure 14 gives examples of that for the case with $\alpha = 0$ and $f_0 = 0.083$ under three triaxialities. The predictions are compared with the results of cell analyses for $a_0/b_0 = 0.5$, i.e. the same value of f_0. The overall agreement in stress response and void volume fraction is quite satisfactory for the lower triaxialities up to $\Sigma_m/\Sigma_e = 1$; the accelerated softening at about $E_e = 0.11$ observed in the cell analyses for $\Sigma_m/\Sigma_e = 1$ is due to strain localization, which is not accounted for in the macroscopic potential. For the triaxiality of $\Sigma_m/\Sigma_e = 3$, however, the void growth after the macroscopic yield point is severely overestimated.

Note that yielding in the macroscopic theory based on (19) implies a rather sudden transition from overall elasticity to overall plastic deformation. The yield stress levels compare favourably with the cell analyses in Fig. 14, but the strains at macroscopic yield are always underestimated. Also notice in Fig. 14(b) that the elastic void volume change prior to yield is quite significant for the higher triaxialities, and is picked up quite well through (21). Incidentally, it is noted that for the present void volume fraction, $f_0 = 0.083$, the effect of porosity on the elastic properties themselves is significant indeed: $E^*/E = 0.85$ according to (22).

The results in Figs 13 and 14 were for materials without strain softening and without strain hardening. Finally, Figs 15 and 16 show the result for two void volume fractions when using the intrinsic softening and hardening parameters that are typical for glassy polymers, and that were used as a reference set in the previous sections (also pressure sensitivity is accounted for, $\alpha = 0.08$). It is seen that for both volume fractions and the various triaxialities, the macroscopic yield points are predicted by (19) with reasonable accuracy, even though significant localization of deformation has already taken place at this point, as discussed before. For stress triaxialities up to 1, the effect of triaxiality on the evolution of the void fraction is also picked up well. At higher triaxialities, the softening due to void growth (in addition to the intrinsic softening of the matrix material) is overestimated considerably, due to the fact that the void growth rate is overestimated. The deviations found here are inevitably connected with the fact that void growth actually takes place by localized flow in the

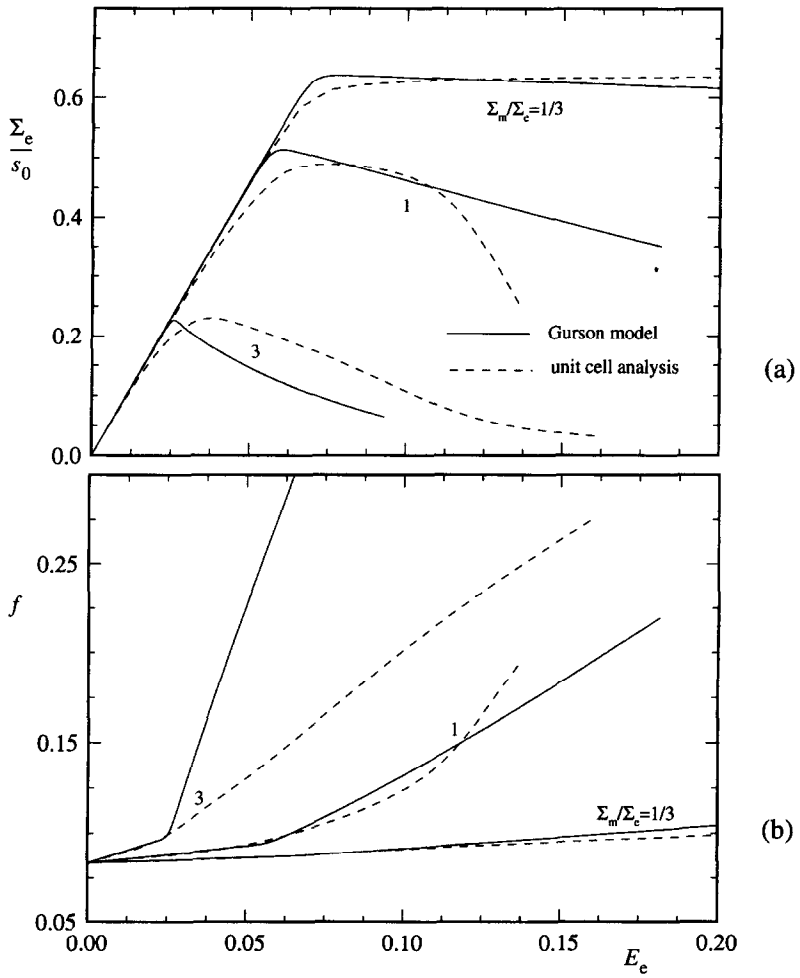

Fig. 14. Comparison between the predictions based on the modified Gurson model and the unit cell results for various remote stress triaxialities. The material constants are $\alpha = 0$, $h/s_0 = 0$ and $C^R/s_0 = 0$, and the initial void is specified by $a_0/b_0 = 0.5$ ($f_0 = 0.083$). (a) Macroscopic effective stress response; (b) evolution of the void volume fraction f.

ligament, while the high triaxiality estimate of the potential is based on spherically symmetric flow around the void.

6. CONCLUSION

The cell model studies reported here have shown that the axisymmetric deformation fields around voids for polymers with softening and subsequent strain hardening can be quite different from those found under similar stress states in metals by, e.g. Needleman (1972), Koplik and Needleman (1988) and Hom and McMeeking (1989).

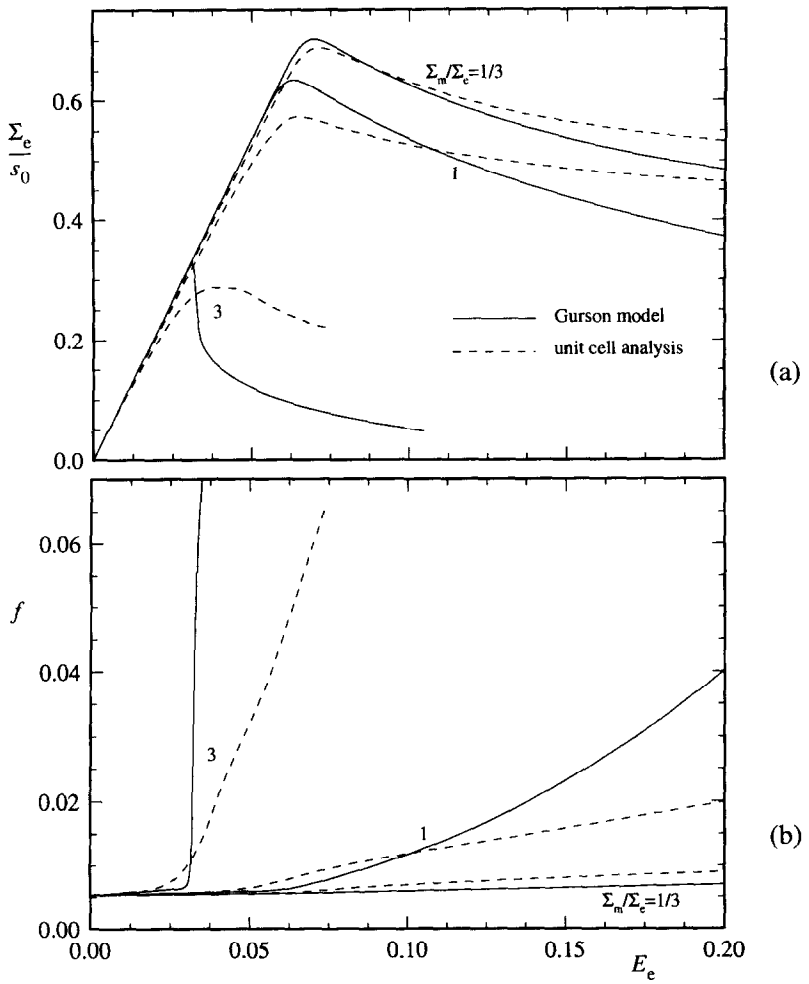

Fig. 15. Comparison between the predictions based on the Gurson model and the unit cell results for various remote stress triaxialities. The material constants are $\alpha = 0.08$, $h/s_0 = 5.15$, $N = 6.3$ and $C^R/s_0 = 0.059$, and the initial void is specified by $a_0/b_0 = 0.2$ ($f_0 = 0.0053$). The unit cell results are from Fig. 8. (a) Macroscopic effective stress response; (b) evolution of the void volume fraction f.

Owing to their typical plastic flow characteristics, void growth in amorphous polymers is controlled typically by the initiation and subsequent propagation of shear bands in the neighbourhood of the void equator (for positive stress triaxialities). Depending primarily on stress triaxiality and to a lesser extent on void volume fraction and material parameters, the shear bands found here belong to one of two types of shear bands, and sometimes a combination of both. It is noted in passing that the shear bands found in a similar plane-strain model (Van der Giessen and Wu, 1995) share some main characteristics with the present findings, but that details of the localized shearing depends on the state of macroscopic deformation. With decreasing intrinsic softening, the tendency for localized shear bands reduces and the deformation

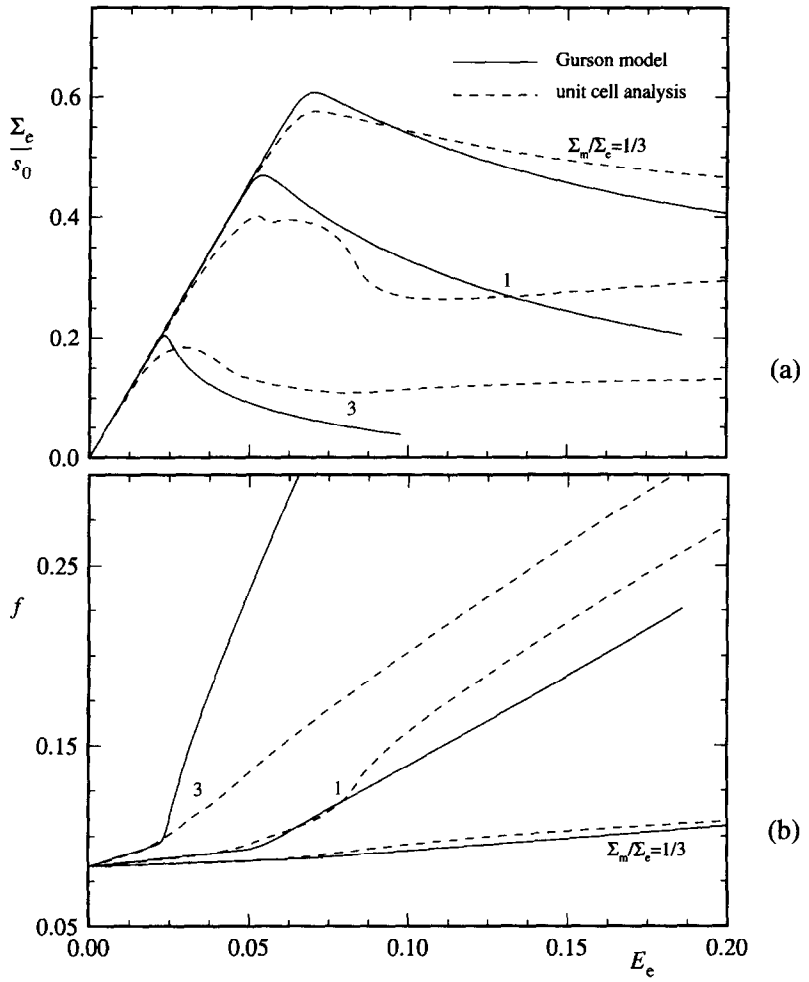

Fig. 16. Comparison between the predictions based on the Gurson model and the unit cell results for various remote stress triaxialities. The material constants are $\alpha = 0.08$, $h/s_0 = 5.15$, $N = 6.3$ and $C^R/s_0 = 0.059$, and the initial void is specified by $a_0/b_0 = 0.5$ ($f_0 = 0.083$). The unit cell results are from Fig. 4. (a) Macroscopic effective stress response; (b) evolution of the void volume fraction f.

becomes more diffuse, just like as found in metals. On the other hand, in both metals and the polymers considered here, progressive void growth leads to necking of the ligament between voids. In metals, where the hardening rate decreases with strain, the ligament necks down (Koplik and Needleman, 1988), whereas in the polymer material we observed drawing of the neck by propagating shear bands.

Void growth studies in elastoplastic polymers have been performed previously (Haward and Owen, 1973; Huang and Kinlock, 1992; Jeong and Pan, 1995), but the shear band features found in the present study have not been obtained in these works. There are probably several reasons for that, but the most important reason is that the finite element meshes used in the referenced previous studies were too coarse to resolve

the fine details of shear bands. Also, the present work has used a recent, more sophisticated constitutive model. Owing to its strain-rate dependence, it allows for shear bands to develop in a stable manner, without a spurious dependence on the mesh size, provided that the mesh is sufficiently refined to resolve the shear bands.

The modified Gurson-type potential proposed here is a step towards a macroscopic constitutive theory for amorphous polymers that are initially porous, for example by previous cavitation of the rubber particles in case of a polymer–rubber blend. In a number of ways, this type of theory needs to be concerned with different aspects than for the application to ductile metals. One of these considered here is the fact that elastic strains cannot be easily neglected as in the case of metals, since the yield strains in polymers are much larger. Also, it should be recalled that the initial void volume fractions are likely to be larger than in metals. Blends typically contain between 10 and 30 vol% rubber particles, and after cavitation the influence of the remaining rubber shell can usually be neglected, so that the initial void volume fractions up to about 10% are not unrealistic. The form considered here is based primarily upon consideration of the macroscopic yield stress, and in this respect its predictions compare reasonably fairly with results of the cell analyses. Several other aspects of the macroscopic response predicted by the macroscopic theory give a rather poor correlation with the cell analyses, especially when the behaviour around the void is controlled by local shear banding. This is an aspect that is typical for amorphous polymers and has not been considered in the many studies of porous ductile metals. Clearly, there is a lot of room for improvement of the theory.

It is noted that yielding as well as intrinsic softening and orientation strain hardening in glassy polymers have been shown experimentally to be temperature and strain-rate dependent (Argon, 1973; Bowden, 1973), but only the influence on yielding is explicitly accounted for in the material model used here. Unfortunately, the effects on softening and orientational hardening are less well understood than those on yielding. It is because of this limitation of the model that we have confined attention here to isothermal deformation processes at a fixed strain-rate. However, especially thermal effects, coupled with the dissipation of energy due to plastic flow, should be expected to be relevant to the types of deformation histories considered here (Boyce *et al.*, 1992; Arruda *et al.*, 1995). A study of this effect on cavity growth will have to await constitutive models that reliably incorporate the temperature dependence of both softening and hardening.

ACKNOWLEDGEMENTS

The work of A. C. Steenbrink is part of a research project funded by the Netherlands Technology Foundation (STW). P. D. Wu is grateful for the Canada International Fellowship granted by the Natural Science and Engineering Research Council of Canada (NSERC).

REFERENCES

Argon, A. S. (1973) A theory for the low-temperature plastic deformation of glassy polymers. *Phil. Mag.* **28,** 839–865.

Arruda, E. M. and Boyce, M. C. (1993) A three-dimensional constitutive model for large stretch behaviour of rubber materials. *J. Mech. Phys. Solids* **41,** 389–412.

Arruda, E. M., Boyce, M. C. and Jayachandran, R. (1995) Effects of strain rate, temperature and thermomechanical coupling on the finite strain deformation of glassy polymers. *Mech. Mater.* **19,** 193–212.

Becker, R. and Needleman, A. (1986) Effect of yield surface curvature on necking and failure in porous plastic solids. *J. Appl. Mech.* **53,** 491–499.

Bowden, P. B. (1973) The yield behaviour of glassy polymers. *The Physics of Glassy Polymers*, ed. R. N. Haward, pp. 279–339. Applied Science Publ., Essex.

Boyce, M. C., Parks, D. M. and Argon, A. S. (1988) Large inelastic deformation of glassy polymers, Part I: rate dependent constitutive model. *Mech. Mater.* **7,** 15–33.

Boyce, M. C., Montagut, E. L. and Argon, A. S. (1992) The effects of thermomechanical coupling on the cold drawing process of glassy polymers. *Polym. Engng Sci.* **32,** 1073–1085.

Bucknall, C. B. (1977) *Toughened Plastics.* Applied Science Publ., London.

Goodier, J. N. (1993) Concentration of stress around spherical and cylindrical inclusions and flaws. *ASME Appl. Mech. Trans.* **55,** 39–44.

Gurson, A. L. (1977) Continuum theory of ductile rupture by void nucleation and growth: Part I. Yield criteria and flow rules for porous ductile media. *J. Engng Mater. Technol.* **99,** 2–15.

Haward, R. N. and Owen, D. R. J. (1973) The yielding of a two-dimensional void assembly in an organic glass. *J. Mater. Sci.* **8,** 1136–1144.

Haward R. N. and Thackray G. (1968) The use of a mathematical model to describe isothermal stress–strain curves in glassy thermoplastics. *Proc. R. Soc. Lond.* **A302,** 453–472.

Hom, C. L. and McMeeking, R. M. (1989) Void growth in elastic–plastic materials. *J. Appl. Mech.* **56,** 309–317.

Huang, Y. and Kinloch, A. J. (1992) Modelling of the toughening mechanisms in rubber-modified epoxy polymers. *J. Mater. Sci.* **27,** 2753–2762.

Huang, Y., Hutchinson, J. W. and Tvergaard, V. (1991) Cavitation instabilities in elastic–plastic solids. *J. Mech. Phys. Solids* **39,** 223–241.

Jeong, H.-Y. and Pan, J. (1995) A macroscopic constitutive law for porous solids with pressure sensitive matrices and its implications to plastic flow localization. *Int. J. Solids Struct.* **32,** 3669–3691.

Koplik, J. and Needleman, A. (1988) Void growth and coalescence in porous plastic solids. *Int. J. Solids Structures* **24,** 835–853.

Lazzeri, A. and Bucknall, C. B. (1993) Dilatational bands in rubber-toughened polymers. *J. Mater. Sci.* **28,** 6799–6808.

Lazzeri, A. and Bucknall, C. B. (1995) Applications of a dilatational yielding model to rubber-toughened polymers. *Polymer* **36,** 2895–2902.

Mear, M. E. and Hutchinson, J. W. (1985) Influence of yield surface curvature on flow localization in dilatant plasticity. *Mech. Mater.* **4,** 395–407.

Needleman, A. (1972) Void growth in an elastic–plastic medium. *J. Appl. Mech.* **39,** 964–970.

Needleman, A., Tvergaard, V. and Van der Giessen, E. (1995) Evolution of void shape and size in creeping solids. *Int. J. Damage Mech.* **4,** 134–152.

Peirce, D., Shih, C. F. and Needleman, A. (1984) A tangent modulus method for rate dependent solids. *Comput. Struct.* **18,** 875–887.

Rice, J. and Tracey, D. M. (1969) On the ductile enlargement of voids in triaxial stress fields. *J. Mech. Phys. Solids* **17,** 210–217.

Sue, H.-J. and Yee, A. F. (1988) Deformation behaviour of a polycarbonate plate with a circular hole: finite elements model and experimental observations. *Polymer* **29,** 1619–1624.

Tandon, G. P. and Weng, G. J. (1988) A theory of particle-reinforced plasticity. *J. Appl. Mech.* **55,** 126–135.

Tvergaard. V. (1981) Influence of voids on shear band instabilities under plane strain conditions. *Int. J. Fract.* **17,** 389–407.

Tvergaard, V. (1982) On localization in ductile materials containing spherical voids. *Int. J. Fract.* **18,** 237–252.

Tvergaard, V. (1990) Material failure by void growth to coalescence. *Adv. Appl. Mech.* **27,** 83–151.

Tvergaard, V. and Van der Giessen, E. (1991) Effect of plastic spin on localization predictions for a porous ductile material. *J. Mech. Phys. Solids* **39,** 763–781.

Van der Giessen, E., Van der Burg, M. W. D., Needleman, A. and Tvergaard, V. (1995) Void growth due to creep and grain boundary diffusion at high triaxialities. *J. Mech. Phys. Solids* **43,** 123–165.

Van der Giessen, E. and Wu, P. D. (1995) Aspects of the plastic deformation in glassy polymer blends. *Mechanics of Plastics and Plastic Composites*, ed. M. C. Boyce, MD-Vol. 68/AMD-Vol. 215, pp. 203–221. ASME, New York.

Worswick, M. J. and Pick, R. J. (1990) Void growth and constitutive softening in a periodically voided solid. *J. Mech. Phys. Solids* **38,** 601–625.

Wu, P. D. and Van der Giessen, E. (1992) On improved 3-D non-Gaussian network models for rubber elasticity. *Mech. Res. Comm.* **19,** 427–433.

Wu, P. D. and Van der Giessen, E. (1993) On improved network models for rubber elasticity and their applications to orientation hardening in glassy polymers. *J. Mech. Phys. Solids* **41,** 427–456.

Wu, P. D. and Van der Giessen, E. (1994) Analysis of shear band propagation in amorphous glassy polymers. *Int. J. Solids Struct.* **31,** 1493–1517.

Wu, P. D. and Van der Giessen, E. (1995a) On neck propagation in amorphous glassy polymers under plane strain tension. *Int. J. Plast.* **11,** 211–235.

Wu, P. D. and Van der Giessen, E. (1996) Computational aspects of localized deformations in amorphous glassy polymers. *Eur. J. Mech.* **15,** 799–823.

APPENDIX

The correction contained in the modified Gurson potential (19) is based on considering the macroscopic yield behaviour of a hollow sphere under hydrostatic loading. The initial outer radius of the sphere is b_0, the radius of the hole is a_0. Finite geometry changes are accounted for, and a and b denote the deformed inner and outer radius, respectively. Loading is applied by way of a prescribed constant expansion rate $\dot{b}/b$, and macroscopic yield is interpreted as the instant where the corresponding hydrostatic stress σ_m attains a maximum. The material of the sphere is taken to be incompressible and to exhibit the elastic–viscoplastic behaviour described in Section 2. However, for convenience, the hyperelastic Hooke's law is used rather than the hypoelastic version in (2) (since the elastic strains remain relatively small, the difference is negligible for the present purpose). Also, as we are mainly interested here in estimating the instant of macroscopic yield, strain softening and hardening are not accounted for in the analysis, i.e. $h = 0$ and $\mathbf{b} = 0$ in the constitutive equations (1)–(8). Pressure dependence of yield is neglected too, i.e. $\alpha = 0$.

Because of spherical symmetry, the problem reduces to a one-dimensional problem in the radial direction, which is formulated here in terms of the radial coordinate r in the current deformed configuration. By virtue of incompressilbity, the deformation field is determined directly through $b^3 - r^3 = b_0^3 - r_0^3$ or $r^3 - a^3 = r_0^3 - a_0^3$, r_0 being the radius in the undeformed configuration. Hence, the overall dilatation $(b/b_0)^3$ is related to the current void volume fraction $f = (a/b)^3$ through

$$\left(\frac{b}{b_0}\right)^3 = \frac{1-f_0}{1-f}.$$

Also then, the rate of deformation can be described completely in terms of the shear rate $\dot{\gamma} = \sqrt{\mathbf{D}\cdot\mathbf{D}}$ [cf. (6)], and expressed in terms of the applied expansion rate $\dot{b}/b$ as

$$\dot{\gamma} = \sqrt{6}\frac{\dot{r}}{r} = \sqrt{6}\frac{\dot{b}}{b}\rho^{-3}, \quad \rho = \frac{r}{b}. \tag{A.1}$$

Integration of (A.1) leads to

$$\gamma = -\sqrt{\frac{2}{3}}\ln\left[1+\left\{\left(\frac{b_0}{b}\right)^3 - 1\right\}\rho^{-3}\right]. \tag{A.2}$$

By incompressibility again, the response of the material is governed solely by the equivalent shear stress τ which can be expressed for this problem as $\tau = (\sigma_\theta - \sigma_r)/\sqrt{3}$, with σ_r and σ_θ denoting the radial and tangential components of Cauchy stress, respectively, in the current deformed configuration at r. Equilibrium requires that

$$\frac{d\sigma_r}{dr} + \frac{2}{r}(\sigma_r - \sigma_\theta) = 0, \tag{A.3}$$

with $\sigma_r(a) = 0$ and $\sigma_r(b) = \sigma_m$. By integration of (A.3), the applied hydrostatic stress can be expressed in terms of the current shear stress distribution inside the sphere as

$$\frac{\sigma_m}{s_0} = 2\sqrt{3}\int_{a/b}^{1}\left(\frac{\tau}{s_0}\right)\frac{d\rho}{\rho}, \tag{A.4}$$

where $\rho = r/b$. It is important to note here that the integral is taken over the deformed configuration. In particular, for small initial void volume fractions, a small macroscopic strain $\ln(b/b_0)$ gives rise to a substantial change in the lower boundary in (A.4).

If the material would be purely elastic, the equivalent shear stress distribution (arbitrarily normalized by s_0) is given by

$$\frac{\tau}{s_0} = c\gamma \quad \text{with } c = \frac{\sqrt{2}}{3}\frac{E}{s_0}. \tag{A.5}$$

Substitution into (A.4) of this distribution with $\gamma = \gamma(\rho)$ from (A.2) leads to an intractable integral that can only be evaluated numerically. For small elastic strains, however, (A.2) reduces to

$$\gamma = \gamma_b\rho^{-3}, \quad \gamma_b = \sqrt{6}\ln(b/b_0),$$

with γ_b the shear strain at $r = b$. In view of the approximations that will be made later on, the application of this strain distribution is sufficiently accurate, as has been checked by numerical calculations. Then, substitution of (A.5) into (A.4) yields the solution for the expansion of an elastic, hollow sphere

$$\frac{\sigma_m}{s_0} = \frac{2}{3}\sqrt{2}c\ln\left(\frac{1-f_0}{1-f}\right)\left(\frac{1}{f}-1\right).$$

Linearization of this solution about f_0 leads to the infinitesimal strain Lamé solution for an incompressible solid [cf. (21)] with $G = E/3$.

If, on the other hand, the material would only deform viscoplastically, one can immediately use the known ρ^{-3}-distribution $\dot{\gamma}(\rho)$ of the shear rate determined by (A.1) to construct the distribution of τ inside the sphere by substituting $\dot{\gamma}$ for $\dot{\gamma}^p$ in (7); i.e. $\tau = \tau(\dot{\gamma}(\rho))$. In the case of an elastic–viscoplastic material, one will in general find a regime $a/b < \rho < p$ where the response is predominantly viscoplastic, while the outer shell $p < \rho < 1$ is still predominantly elastic. This

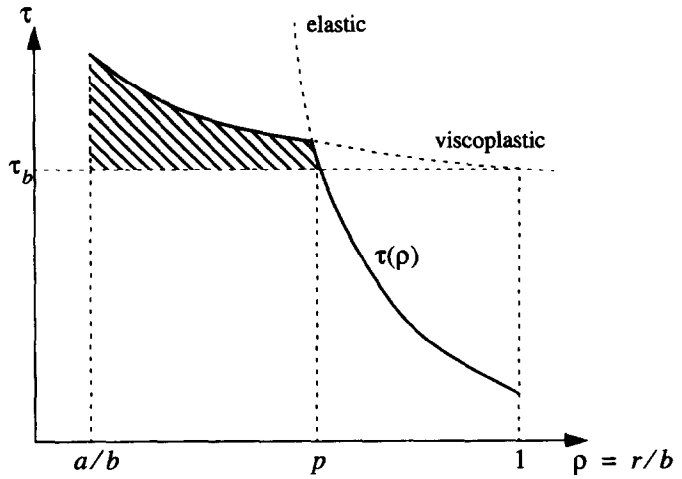

Fig. A1. Schematic distribution of the equivalent shear stress τ in an elastic–viscoplastic sphere of radius b with void of radius a under hydrostatic loading. In deriving (A.6), the stress distribution inside the plastic zone $a/b < \rho < p$ is approximated by a uniform stress level τ_b, thus neglecting the dashed area.

is shown schematically in Fig. A1. As the transition between the two regions for the kind of viscoplastic behaviour considered here is very sharp, the idea of a plastic front is meaningful. The position $\rho = p$ of the current plastic front can be approximated by equating the elastic shear stress distribution with the viscoplastic shear stress $\tau_b = \tau(\dot{\gamma}_b)$ at the outer radius of the sphere (see Fig. A1)

$$c\gamma_b p^{-3} = \tau_b/s_0.$$

Then, the integral expression (A.4) can be approximated by assuming a uniform stress τ_b inside the plastic zone and the elastic distribution outside, and one obtains

$$\frac{\sigma_m}{s_0} = 2\sqrt{3}\frac{\tau_b}{s_0}\left[\int_{a/b}^{p}\frac{d\rho}{\rho} + \int_{p}^{1}\left(\frac{p}{\rho}\right)^3\frac{d\rho}{\rho}\right]$$

$$= \frac{2}{\sqrt{3}}\frac{\tau_b}{s_0}[\ln(p^3/f) + 1 - p^3]. \tag{A.6}$$

The yield stress of the porous material is defined as the instant where the macroscopic stress σ_m attains its maximum value Σ_m. A closed-form analytical expression for the yield stress Σ_m according to (A.6) has not been found, but it turned out that the numerical solution could be fitted to a fair accuracy by the expression

$$\frac{\Sigma_m}{s_0} = \frac{2}{\sqrt{3}}\frac{\tau_b}{s_0}e\left[\exp\left(-\frac{1}{e}\ln f_0\right) - 1\right]. \tag{A.7}$$

The parameter e has been determined by maximization of (A.6) for the limiting case of a void in an infinite matrix, $f_0 \to 0$. Then we find

$$e = \ln\left(\frac{3\sqrt{3}}{2}\frac{\tau_b/s_0}{E/s_0}\right) + 1 \approx \ln(\tau_b/E).$$

Now, in the limiting case that elasticity can be neglected, $\tau_b/E \to 0$, as relevant for instance for ductile metals, we have $e \to -\infty$. Then, the value of Σ_m according to (A.7) reduces to the

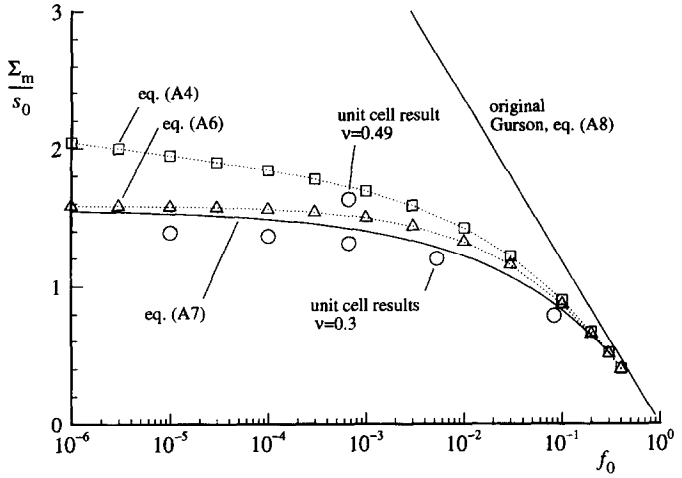

Fig. A2. Comparison of the elasto-viscoplastic estimate (A.7) for the hydrostatic yield stress Σ_m as a function of the initial void volume fraction f_0 with (i) numerical results based on (A.6) or on (A.4), and (ii) results from finite element cell analyses. Also shown is the result according to the original Gurson yield condition (A.8).

hydrostatic stress at yield according to the Gurson yield function (17) under a purely hydrostatic state of stress

$$\frac{\Sigma_m}{s_0} = \frac{2}{\sqrt{3}}\frac{\tau_b}{s_0}\operatorname{arccosh}\left(\frac{1+f_0^2}{2f_0}\right) = -\frac{2}{\sqrt{3}}\frac{\tau_b}{s_0}\ln f_0, \tag{A.8}$$

which is indeed based on full rigid-plastic flow throughout the sphere (Gurson, 1977).

In order to verify the accuracy of the approximate expression (A.7), its predicted macroscopic yield stresses are shown in Fig. A2 for a wide range of initial void volume fractions. The results are compared to predictions based on integration of the actual stress field, according to (A.4), and on the approximation according to (A.6). First of all, it is seen that (A.7) agrees very well with the results obtained numerically from the approximate stress distribution (A.6). These solutions, in turn, are in good agreement with the full numerical solution based on (A.4) for initial volume fractions larger than 10^{-2} or so, but tend to deviate somewhat for $f_0 \to 0$. This is caused by the fact that for small void volume fractions the strain rate and yield stress at the inner radius are much larger than at the outer radius, so that the error in deriving (A.6) by neglecting the hatched area in Fig. A1 becomes more significant for small void volume fractions. For this reason, (A.6) underestimates the macroscopic yield stress. It is noted, however, that for the application of the model to porous polymeric materials and to polymer–rubber blends, the range of significant void volume fractions is roughly from 1 to 30%. Within this range, the accuracy of (A.6)–(A.7) compared to (A.4) is acceptable.

The predictions are also confronted with finite element unit cell analyses under purely hydrostatic states of remote stress assuming the same elastic–viscoplastic material behaviour ($h = \alpha = 0$, $\mathbf{b} = 0$) as discussed in Section 5.2. Based on the above observations, one would expect that (A.6) and (A.7) underestimate the cell results. The reason that this is not found (see Fig. A2), is that the cell analyses have accounted for elastic compressibility by using $\nu = 0.3$. This has a significant effect, as is illustrated in Fig. A2, by showing for $f_0 = 10^{-3}$ also the result for nearly incompressible material ($\nu = 0.49$). In that case, the result of the cylindrical cell model is very close to the analytical result for the spherical model (A.4). Thus, the good agreement seen in Fig. A2 between the unit cell results and the simple estimate (A.7) is to some extent due to two approximations partially cancelling each other. Nevertheless, the approximation offered by (A.7) is much better than that of the original Gurson result (A.8)

for smaller values of f_0. For sufficiently large f_0, the plastic zone extends over the major part of the sphere, and the present elastic–viscoplastic estimate approaches to that from Gurson's model. Differences between the two estimates at small f_0 originate partly from elasticity effects and partly from the fact that the present estimate accounts for finite strain geometry changes. The latter is primarily responsible for (A.7) predicting a finite limiting value of Σ_m for $f_0 \to 0$ (this tendency is confirmed by the unit cell results as well as by the numerical solution based on (A.4), although the actual values of this limit value differ somewhat). This feature of the result (A.7) is suggestive of the possibility of cavitation instabilities [see e.g. Huang *et al.* (1991)]; but, this is outside the scope of this paper, and will be considered separately in another paper.